

# COSMOLOGICAL IMPLICATIONS OF LARGE-SCALE FLOWS<sup>1</sup>

Avishai Dekel

Racah Institute of Physics, The Hebrew University, Jerusalem 91904, Israel  
and University of California, Berkeley & Santa Cruz

## ABSTRACT

Cosmological implications of the observed large-scale peculiar velocities are reviewed, alone or combined with redshift surveys and CMB data. The latest version of the POTENT method for reconstructing the underlying three-dimensional velocity and mass-density fields is described. The initial fluctuations and the nature of the dark matter are addressed via statistics such as bulk flow and mass power spectrum. The focus is on constraining the mass density parameter  $\Omega$ , directly or via the parameter  $\beta$  which involves the unknown relation between galaxies and mass. The acceptable range for  $\Omega$  is found to be 0.4 – 1.0. The range of  $\beta$  estimates is likely to reflect non-trivial features in the galaxy biasing scheme, such as scale dependence. Similar constraints on  $\Omega$  and  $\Lambda$  from global measures are summarized.

## 1. INTRODUCTION

A major goal of the analysis of cosmic flows is measuring the cosmological parameters, in particular the mass density parameter,  $\Omega$  (or  $\Omega$ ). As illustrated in Figure 1, the data can be used to constrain  $\Omega$  in several different ways. Methods that are based on the peculiar velocity data alone (§ 4) are independent of the “biasing” relation between galaxy and mass density. They refer to the present-day large-scale structure (LSS) which is insensitive to the cosmological constant  $\Lambda$ . They can thus serve to measure  $\Omega$  directly, but they involve relatively large errors. These methods largely rely on the assumption (supported by observations, *e.g.*, Nusser, Dekel & Yahil 1995) that the initial fluctuations were drawn from a *Gaussian* random field.

All the methods that use the spatial distribution of galaxies must depend on the biasing relation between the densities of galaxies and mass. In the linear approximation to gravitational instability theory (GI), which is roughly valid for the fields when they are smoothed on very large scales, what is actually being measured by these methods is the degenerate

---

<sup>1</sup>in “Galaxy Scaling Relations: Origins, Evolution and Applications”, ed. L. da Costa (Springer) in press (1997). A more complete discussion is in “Formation of Structure in the Universe”, eds. A. Dekel & J.P. Ostriker (Cambridge University Press) in press (1997).

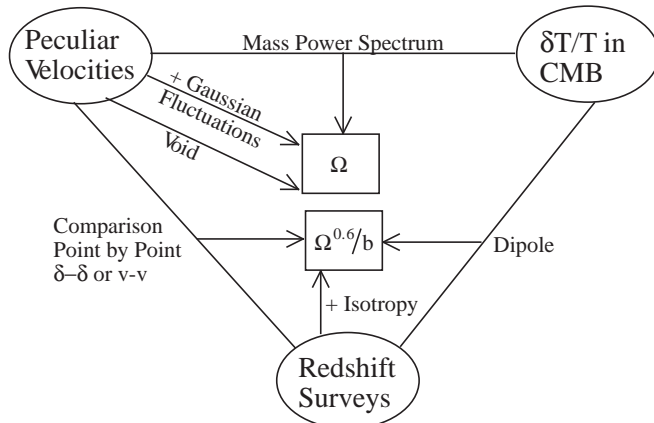


Fig. 1.— Methods for measuring  $\Omega$  and  $\beta$  from large-scale flows.

parameter  $\beta \equiv \Omega^{0.6}/b$  rather than  $\Omega$  itself, where the density fluctuations of galaxies and mass are assumed to be related via a linear biasing relation,  $\delta_G = b\delta$ . These methods include, for example, measurements of redshift-space distortions from redshift surveys under the assumption of global isotropy, comparisons of the galaxy distribution with the CMB dipole, and comparisons of the observed peculiar velocities with the galaxy distribution (or the predicted velocities) deduced from redshift surveys (§ 5). The most recent best estimates of  $\beta$  for IRAS galaxies lie in the range  $0.5 \leq \beta_I \leq 0.9$ . As argued below, the contamination by non-trivial biasing introduces a significant uncertainty in the translation of the various  $\beta$  estimates to a reliable measurement of  $\Omega$ .

Another way of determining  $\Omega$  is by comparing the mass power spectrum from observed peculiar velocities with the spectrum of fluctuations in the CMB (§ 3.3, § 3.4). This comparison involves more detailed modeling of the formation of structure, and the current studies are limited to the CDM family of models, allowing for a non-zero cosmological constant, a possible tilt in the spectrum with or without tensor fluctuations, and a mixture of dark-matter species.

The outline is as follows: § 2 briefly describes reconstruction methods from peculiar velocities. § 3 discusses the statistics of mass-density fluctuations, including bulk flow and power spectrum, as determined by the velocity data alone or combined with CMB data. § 4 focuses on direct estimates of  $\Omega$  from peculiar velocities alone. § 5 presents estimates of  $\beta$  by comparing velocity and galaxy density data, and addresses the issue of biasing. § 6 puts the results in perspective by summarizing other measures of the cosmological parameters. § 6.1 provides a summary of the results.

## 2. POTENT RECONSTRUCTION FROM PECULIAR VELOCITIES

## 2.1. Data for Velocity Analysis

The key for measuring peculiar velocities are the distance indicators (for review: Willick 1997). The current typical intrinsic scattering the Tully-Fisher (TF) distance indicator is at best  $\sigma_m \sim 0.33$  mag, corresponding to a relative distance error of  $\Delta = (\ln 10/5)\sigma_m \approx 0.15$ .

The most comprehensive catalog of peculiar velocity data available today is the Mark III catalog (Willick *et al.* 1995; 1996; 1997a), which is a careful compilation of several data sets under the assumption that all galaxies trace the same underlying velocity field. The merger was non-trivial because the observers differ in their selection procedure, the quantities they measure, the method of measurement and the TF calibration techniques.

The original Mark II catalog, which was used in the first application of POTENT (Dekel *et al.* 1990; Bertschinger *et al.* 1990), consisted of about 1000 galaxies (mostly Lynden-Bell *et al.* 1988 and Aaronson *et al.* 1982). The extended Mark III catalog consists of  $\sim 3400$  galaxies (dominated by Mathewson *et al.* 1992). This sample enables a reasonable recovery of the dynamical fields with  $12 h^{-1}\text{Mpc}$  smoothing in a sphere of radius  $\sim 60 h^{-1}\text{Mpc}$  about the Local Group (LG), extending to  $\sim 80 h^{-1}\text{Mpc}$  in certain regions (§ 2.7). More uniformly sampled data of more than 1000 spiral galaxies in the north is in preparation, and was already subject to preliminary analysis (SFI, Giovanelli *et al.* 1997).

## 2.2. Methods of Velocity Analysis

One way of classifying the methods of velocity analysis is as follows:

	Inferred Distance Space	Redshift-Space + V Model
Forward TF	POTENT <i>selection + distance bias</i>	VELMOD <i>selection bias</i>
Inverse TF	POTINV <i>distance bias</i>	MFPOT <i>z-space smoothing</i>

The “forward” and “inverse” methods refer to whether the TF relation is interpreted as  $M(\eta)$  or  $\eta(M)$  ( $M$  being the absolute magnitude and  $\eta$  the rotation velocity). The difference is crucial because the apparent magnitude depends on distance while  $\eta$  is not, and because the selection depends on magnitude and is independent of  $\eta$ . On the other hand, the velocity field can be computed either from peculiar velocities that were evaluated at each galaxy’s TF-inferred position,  $\mathbf{d}$ , or by fitting a parametric model for the potential (and thus the velocity) field in redshift space,  $\mathbf{z}$ . Each method is affected by different systematic errors, and techniques have been developed for statistically correcting them. The success of each technique has been tested using mock catalogs, and the goal is to have the different methods recover consistent results.

The original POTENT described below is a *forward* TF method in d-space. It has to deal with *selection* bias of the TF parameters because of the magnitude limit, and with *Malmquist* bias in the inferred distances and velocities arising from the random distance

errors convolved with the geometry of space and the clumpiness of the galaxy distribution. Methods have been developed for statistically correcting these biases. In particular, the correction of the Malmquist bias requires external information about the underlying number density of galaxies in the samples from which galaxies were selected for the peculiar velocity catalogs (see Willick 1997).

One can alternatively infer distances using the *inverse* TF relation. This eliminates the selection bias, but there is still an inferred-distance Malmquist bias. In the inverse-TF case, the distance bias can in principle be corrected using information that is fully contained in the catalog itself (Landy & Szalay 1992). In practice, the quality of the correction is limited by the sparseness of the sampling. The POTENT analysis of the inverse data corrected this way is termed POTINV (Eldar, Dekel & Willick 1997).

If the selection does not explicitly depend on  $\eta$ , Malmquist bias can be eliminated by minimizing  $\eta$  residuals in redshift space without ever inferring actual distances to individual galaxies. The distance is replaced by  $r = z - u_\alpha(z)$ , where  $u_\alpha$  is a parametric model for the radial peculiar velocity field. If the forward TF relation is used, as in VELMOD (Willick *et al.* 1997b; § 5.4), the method still has to correct for selection bias. The use of the *inverse* TF relation (Schechter 1980) guarantees in this case that both the selection bias and the distance bias are eliminated, at the expense of over-smoothing due to the representation of the fields in redshift space. Recent implementations of such methods were termed MF POT (Blumenthal, Dekel & Yahil 1997) and ITF (Davis, Nusser, & Willick 1996).

Another way of distinguishing between the methods is by their goals. The methods working in d-space can serve for reconstruction of 3D maps of the velocity and mass-density fields, unbiased and uniformly smoothed with equal-volume weighting throughout the volume. These fields can then be straightforwardly compared to other data and to theory in order to obtain cosmological implications (*e.g.*, § 5.2). Alternatively, one may direct the method to estimating certain parameters of the model (*e.g.*,  $\beta$ ) without ever reconstructing uniform maps. The redshift-space methods serve this purpose well (*e.g.*, § 5.4).

Yet another characteristic of some of the methods is the usage of a whole-sky redshift survey (such as IRAS 1.2 Jy) as an intrinsic part of the reconstruction from peculiar velocities. This is the case in the SIMPOT, VELMOD and ITF methods (§ 5). These methods are geared towards determining  $\beta$ , with SIMPOT also providing uniform reconstruction maps.

Finally, one can focus on optimal formal treatment of the random errors, which are in fact the main obstacle. A method based on Wiener Filtering has been developed for recovering the most probable mean field from the noisy peculiar-velocity data in d-space (Zaroubi, Dekel & Hoffman, in preparation). This can serve as a basis for constrained realizations of uniform smoothing, each of which being an equally good guess for the structure in our real cosmological neighborhood.

### 2.3. Correcting Malmquist Bias

The selection bias in the calibration of the forward TF relation can be corrected once the selection function is known (see Willick 1994). But then, the TF inferred distance,  $d$ , and the mean peculiar velocity at a given  $d$ , suffer from a *Malmquist* or *inferred-distance* bias. The distances, either forward or inverse, are corrected for Malmquist bias in a statistical way before being fed as input to POTENT-like procedures.

If  $M$  is distributed normally for a given  $\eta$ , with standard deviation  $\sigma_m$ , then the forward inferred distance  $d$  of a galaxy at a true distance  $r$  is distributed log-normally about  $r$ , with relative error  $\Delta \approx 0.46\sigma_m$ . Given  $d$ , the expectation value of  $r$  is

$$E(r|d) = \frac{\int_0^\infty r P(r|d) dr}{\int_0^\infty P(r|d) dr} = \frac{\int_0^\infty r^3 n(r) \exp\left(-\frac{[\ln(r/d)]^2}{2\Delta^2}\right) dr}{\int_0^\infty r^2 n(r) \exp\left(-\frac{[\ln(r/d)]^2}{2\Delta^2}\right) dr}, \quad (1)$$

where  $n(r)$  is the number density in the underlying distribution from which galaxies were selected. The deviation of  $E(r|d)$  from  $d$  reflects the bias. The homogeneous part arises from the geometry of space — the inferred distance  $d$  underestimates  $r$  because it is more likely to have been scattered by errors from  $r > d$  than from  $r < d$ , the volume being  $\propto r^2$ . If  $n = \text{const}$ , equation 1 reduces to  $E(r|d) = de^{3.5\Delta^2}$ , in which the distances should simply be multiplied by a factor, 8% for  $\Delta = 0.15$ , equivalent to changing the zero-point of the TF relation. Fluctuations in  $n(r)$  are responsible for the inhomogeneous bias (IM), which systematically enhances the inferred density perturbations and thus the value of  $\Omega$  inferred from them.

In one version of the Mark III data for POTENT analysis, the forward IM bias is corrected in two steps. First, the galaxies are grouped in  $z$ -space (Willick *et al.* 1995), reducing the distance error of each group of  $N$  members to  $\Delta/\sqrt{N}$  and thus significantly weakening the bias. With or without grouping, the noisy inferred distance of each object,  $d$ , is replaced by  $E(r|d)$ , with an assumed  $n(r)$  properly corrected for grouping if necessary. This procedure has been tested using realistic mock data from N-body simulations, showing that IM bias can be reduced to the level of a few percent. The practical uncertainty is in  $n(r)$ , which can be approximated for example by the high-resolution density field of IRAS or optical galaxies, or by the recovered mass-density itself in an iterative procedure under certain assumptions about how galaxies trace mass. The resultant correction to the density recovered by POTENT is  $< 20\%$  even at the highest peaks.

Distances are alternatively inferred via the *inverse* TF relation between internal velocity parameter  $\eta$  and magnitude  $m$ ,  $\eta = \eta^0(m - 5 \log d)$ . Under the assumption that the selection was independent of  $\eta$  and was not an explicit function of distance, the expectation value of the true distance  $r$  given  $d$  is

$$E(r|d) = d e^{3\Delta^2/2} f(de^{\Delta^2})/f(d), \quad (2)$$

where  $\Delta \equiv (\ln 10/5)\sigma_\eta/\eta^0$ . In this case, the required density function,  $f(d)$ , is in  $d$ -space, and is derivable from the sample itself (Landy & Szalay 1992). Eldar, Dekel & Willick

(1997) have applied this correction to the inverse distances in the Mark III catalog, to serve as input for a POTENT analysis (POTINV). The agreement between the forward POTENT and POTINV results are well within the level of the random errors.

## 2.4. Smoothing the Radial Velocities

The goal of the POTENT analysis is to recover from the collection of Malmquist-corrected, radial peculiar velocities  $u_i$  at inferred positions  $\mathbf{d}_i$  the underlying 3D velocity field  $\mathbf{v}(\mathbf{x})$  and the associated mass-density fluctuation field  $\delta(\mathbf{x})$ , smoothed with a Gaussian of radius  $R_s$  (we denote hereafter a 3D Gaussian window of radius  $12 h^{-1}\text{Mpc}$  by G12, etc.). The first, most difficult step is the smoothing, or interpolation, into a radial velocity field with minimum bias,  $u(\mathbf{x})$ . The desire is to reproduce the  $u(\mathbf{x})$  that would have been obtained had the true  $\mathbf{v}(\mathbf{x})$  been sampled densely and uniformly and smoothed with a spherical Gaussian window of radius  $R_s$ . With the data as available,  $u(\mathbf{x}_c)$  is taken to be the value at  $\mathbf{x} = \mathbf{x}_c$  of an appropriate *local* velocity model  $\mathbf{v}(\alpha_k, \mathbf{x} - \mathbf{x}_c)$ . The model parameters  $\alpha_k$  are obtained by minimizing the weighted sum of residuals,

$$S = \sum_i W_i [u_i - \hat{\mathbf{x}}_i \cdot \mathbf{v}(\alpha_k, \mathbf{x}_i)]^2, \quad (3)$$

within an appropriate local window  $W_i = W(\mathbf{x}_i, \mathbf{x}_c)$ . The window is a Gaussian, modified such that it minimizes the combined effect of the following three types of errors.

**Tensor window bias.** Unless  $R_s \ll r$ , the  $u_i$ s cannot be averaged as scalars because the directions  $\hat{\mathbf{x}}_i$  differ from  $\hat{\mathbf{x}}_c$ , so  $u(\mathbf{x}_c)$  requires a fit of a local 3D model as in Eq. 3. The original POTENT used the simplest local model,  $\mathbf{v}(\mathbf{x}) = \mathbf{B}$  of 3 parameters, for which the solution can be expressed explicitly in terms of a tensor window function (Dekel *et al.* 1990). However, a bias occurs because the tensorial correction to the spherical window has conical symmetry, weighting more heavily objects of large  $\hat{\mathbf{x}}_i \cdot \hat{\mathbf{x}}_c$ . A way to reduce this bias is by generalizing the zeroth-order  $\mathbf{B}$  into a 9-parameter first-order velocity model,  $\mathbf{v}(\mathbf{x}) = \mathbf{B} + \bar{\mathbf{L}} \cdot (\mathbf{x} - \mathbf{x}_c)$ , with  $\bar{\mathbf{L}}$  a symmetric tensor that automatically ensures local irrotationality. The linear terms tend to “absorb” most of the bias, leaving  $\mathbf{v}(\mathbf{x}_c) = \mathbf{B}$  less biased. Unfortunately, a high-order model tends to pick undesired small-scale noise. The optimal compromise for the Mark III data was found to be a 9-parameter model fit out to  $r = 40 h^{-1}\text{Mpc}$ , smoothly changing to a 3-parameter fit beyond  $60 h^{-1}\text{Mpc}$  (Dekel *et al.* 1997).

**Sampling-gradient bias.** If the true velocity field is varying within the effective window, the non-uniform sampling introduces a bias because the smoothing is galaxy-weighted whereas the aim is equal-volume weighting. The simplest way to correct this bias is by weighting each object with the local volume that it “occupies”, or the inverse of the local density. A crude estimate of this volume is  $V_i \propto R_n^3$ , where  $R_n$  is the distance to the  $n$ -th neighboring object (*e.g.*,  $n = 4$ ). This procedure is found via simulations to reduce the sampling-gradient bias in Mark III to negligible levels typically out to  $60 h^{-1}\text{Mpc}$  as long as one keeps out of the Galactic zone of avoidance. The  $R_n(\mathbf{x})$  field can serve later as a flag for poorly sampled regions, to be excluded from any quantitative analysis.

**Reducing random errors.** The ideal weighting for reducing the effect of Gaussian noise has weights  $W_i \propto \sigma_i^{-2}$ , where  $\sigma_i$  are the distance errors. Unfortunately, this weighting spoils the carefully designed volume weighting, biasing  $u$  towards its values at smaller  $r_i$  and at nearby clusters where the errors are small. A successful compromise is to weight by both, *i.e.*

$$W(\mathbf{x}_i, \mathbf{x}_c) \propto V_i \sigma_i^{-2} \exp[-(\mathbf{x}_i - \mathbf{x}_c)^2 / 2R_s^2] . \quad (4)$$

The resultant errors in the recovered fields are assessed by Monte-Carlo simulations. We generate noisy data via full, realistic Monte-Carlo mock catalogs, where the noise is added as scatter in the TF quantities (Kolatt *et al.* 1996). The error in the final  $\delta$  at a grid point is estimated by the standard deviation of the recovered  $\delta$  over the Monte-Carlo simulations,  $\sigma_\delta$  (and similarly  $\sigma_v$ ). In the well-sampled regions, which extend in Mark III out to 40–60  $h^{-1}$ Mpc, the errors are  $\sigma_\delta \approx 0.1$ –0.3, but they may blow up in certain regions at large distances. To exclude noisy regions, any quantitative analysis could be limited to points where  $\sigma_v$  and  $\sigma_\delta$  are within certain bounds.

## 2.5. From Radial Velocity to Density Fields

If the LSS evolved according to GI, then the large-scale velocity field is expected to be *irrotational*,  $\nabla \times \mathbf{v} = 0$ . Any vorticity mode would have decayed during the linear regime as the universe expanded, and, based on Kelvin’s circulation theorem, the flow remains vorticity-free in the mildly-nonlinear regime as long as it is laminar. Bertschinger & Dekel (1989) have demonstrated that irrotationality is valid to a good approximation when a nonlinear velocity field is properly smoothed over. Irrotationality implies that the velocity field can be derived from a scalar potential,  $\mathbf{v}(\mathbf{x}) = -\nabla\Phi(\mathbf{x})$ , so the radial velocity field  $u(\mathbf{x})$  should contain in principle enough information for a full 3D reconstruction. In the POTENT procedure, the potential is computed by integration along radial rays from the observer,

$$\Phi(\mathbf{x}) = - \int_0^r u(r', \theta, \phi) dr' . \quad (5)$$

The two missing transverse velocity components are then recovered by differentiation.

The final step of the POTENT procedure is the derivation of the mass-density fluctuation field associated with the peculiar velocity field. This requires a solution to the equations of GI in the mildly-nonlinear regime with mixed boundary conditions.

Let  $\mathbf{x}, \mathbf{v}$  be the position and peculiar velocity in comoving units (corresponding to  $a\mathbf{x}$  and  $a\mathbf{v}$  in physical units, with  $a(t)$  the universal expansion factor). Let  $\delta \equiv (\rho - \bar{\rho})/\bar{\rho}$  be the mass-density fluctuation. The equations governing the evolution of fluctuations of a pressureless gravitating fluid in a standard cosmological background during the matter era are the *Continuity* equation, the *Euler* equation of motion, and the *Poisson* field equation.

In the *linear* approximation, the growing mode of the solution,  $\delta \propto D(t)$ , is irrotational and can be expressed in terms of  $f(\Omega) \equiv H^{-1}\dot{D}/D \approx \Omega^{0.6}$ . The corresponding linear relation between density and velocity is  $\delta_1 = -f^{-1}\nabla \cdot \mathbf{v}$ . The use of  $\delta_1$  is limited to the small

dynamical range between a few tens of megaparsecs and the  $\sim 100 h^{-1}\text{Mpc}$  extent of the current samples. However, the sampling of galaxies enables reliable dynamical analysis with a smoothing radius as small as  $\sim 10 h^{-1}\text{Mpc}$ , where  $|\nabla \cdot \mathbf{v}|$  obtains values larger than unity and therefore nonlinear effects play a role. Even reconstruction with  $\sim 5 h^{-1}\text{Mpc}$  smoothing may be feasible in well-sampled regions nearby. Figure 2 shows that  $\delta_1$  becomes a severe underestimate at large  $|\delta|$ . Mild nonlinear effects carry crucial information about the formation of LSS, and should therefore be treated properly.

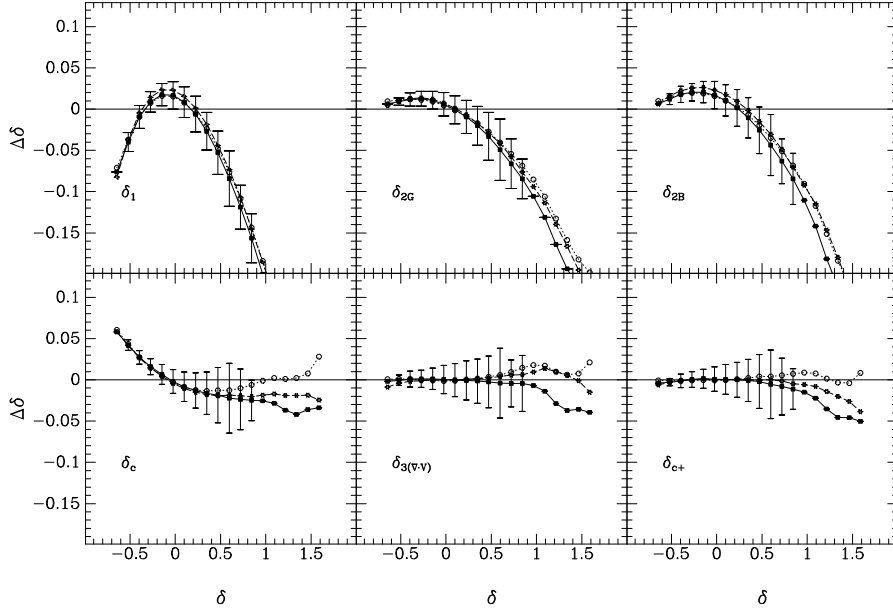


Fig. 2.— Quasi-linear velocity-to-density approximations.  $\Delta\delta \equiv \delta_{approx}(\mathbf{v}) - \delta_{true}$ . The mean and standard deviation are from large CDM N-body simulations normalized to  $\sigma_8 = 1$ , smoothed G12. The three curves correspond to different models: standard CDM (squares, solid), tilted CDM ( $n = 0.6$ , stars, dashed), and open CDM ( $\Omega = 0.2$ , open circles, dotted) (Ganon *et al.* 1997).

A basis for useful *mildly-nonlinear* relations is provided by the Zel’dovich (1970) approximation. The displacements of particles from their initial, Lagrangian positions  $\mathbf{q}$  to their Eulerian positions  $\mathbf{x}$  at time  $t$  are assumed to have a universal time dependence, and thus,  $\mathbf{x}(\mathbf{q}) - \mathbf{q} = f(\Omega)^{-1}\mathbf{v}(\mathbf{q})$ . For the purpose of approximating GI, the Lagrangian Zel’dovich approximation can be interpreted in *Eulerian* space,  $\mathbf{q}(\mathbf{x}) = \mathbf{x} - f^{-1}\mathbf{v}(\mathbf{x})$ , provided that the flow is *laminar* with no orbit mixing, or when multi-streams are appropriately smoothed over. The solution of the continuity equation then yields (Nusser *et al.* 1991)

$$\delta_c(\mathbf{x}) = \|I - f^{-1}\partial\mathbf{v}/\partial\mathbf{x}\| - 1, \quad (6)$$

where the bars denote the Jacobian determinant and  $I$  is the unit matrix. The Zel’dovich displacement is first order in  $f^{-1}$  and  $\mathbf{v}$  and therefore the determinant in  $\delta_c$  includes second- and third-order terms as well, involving sums of double and triple products of partial derivatives which we term  $\Delta_2(\mathbf{x})$  and  $\Delta_3(\mathbf{x})$  respectively.



The approximation  $\delta_c$  can be improved by slight adjustments of the coefficients of the  $n$ th-order terms,

$$\delta_{c+} = -(1 + \epsilon_1)f^{-1}\nabla\cdot\mathbf{v} + (1 + \epsilon_2)f^{-2}\Delta_2 + (1 + \epsilon_3)f^{-3}\Delta_3 . \quad (7)$$

The coefficients were empirically tuned to best fit the CDM simulation of  $12 h^{-1}\text{Mpc}$  smoothing over the whole range of  $\delta$  values, with  $\epsilon_1 = 0.06$ ,  $\epsilon_2 = -0.13$  and  $\epsilon_3 = -0.3$ . This approximation is found to be robust to uncertain features such as the value of  $\Omega$ , the shape of the power spectrum, and the degree of non-linearity as determined by the fluctuation amplitude and the smoothing scale. Such robustness is crucial when a quasilinear approximation is used for determining  $\Omega$  (§ 4). This is the approximation currently used in POTENT.

Fig. 2 compares the accuracy of the various approximations using the N-body simulations.  $\delta_c$  is the best among the physically motivated approximations, which also include two second-order approximations (Bernardeau 1992; Gramman 1993). The latter do somewhat better at the negative tail, but they provide severe underestimates in the positive tail.  $\delta_{c+}$  is an excellent robust fits over the whole mildly-nonlinear regime.

We note in passing that the relation 6 is not easily invertible to solve for  $\mathbf{v}$  when  $\delta$  is given, *e.g.*, from redshift surveys, but a useful approximation derived from simulations is  $\nabla\cdot\mathbf{v} = -f\delta/(1 + 0.18\delta)$ .

## 2.6. Testing with Mock Catalogs

The way to optimize POTENT and other reconstruction methods is by minimizing the systematic errors when applied to mock catalogs. It is important that these mock catalogs mimic the real data as closely as possible. Such mock catalogs have been produced, for example, to mimic the Mark III and the IRAS 1.2Jy catalogs (Kolatt *et al.* 1996). They are publically available and serve as standard “benchmarks” for the competing methods.

The procedure for making these mock catalogs involves two main steps: a dynamical N-body simulation that mimics our actual cosmological neighborhood, and the generation of galaxy catalogs from it.

Figure 3 demonstrate the quality of the POTENT reconstruction from the Mark III catalog by comparing the recovered density field to the true G12-smoothed field. This comparison is done at the points of a uniform grid inside a volume of effective radius  $40 h^{-1}\text{Mpc}$ . The field shown is the average of the fields recovered from ten Monte Carlo mock catalogs of noisy galaxy velocities sampled sparsely and nonuniformly. One can see that the remaining systematic errors are small. The final systematic error is not correlated with the signal (slope  $\sim$ unity in the scatter diagram) and is on the order of  $\Delta\delta \sim 0.13$ . The random errors are not a major obstacle in certain well-sampled regions (such as the Great Attractor), but they become severe in poorly-sampled regions (such as parts of the Perseus-Pisces region near the Galactic plane). The errors derived from the noisy mock catalogs are used to eliminate poorly-recovered regions from quantitative analyses.

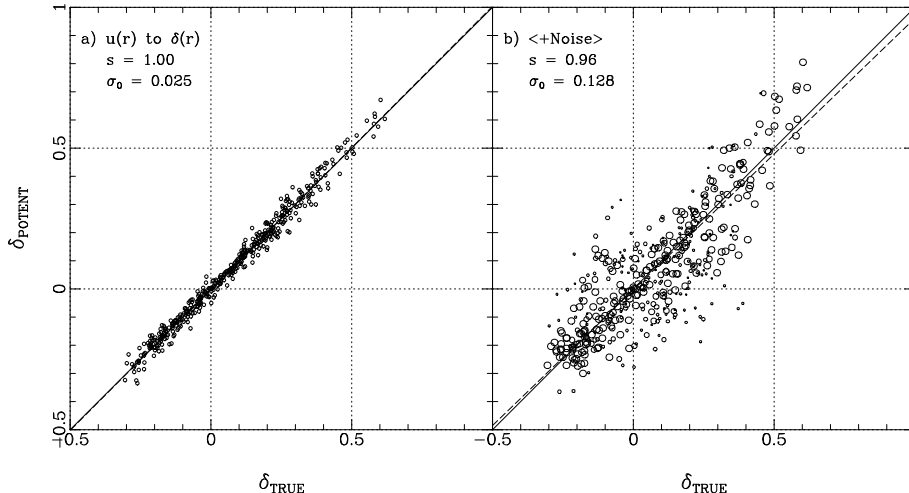


Fig. 3.— Systematic errors in the POTENT analysis. The density field recovered by POTENT from the mock data is compared with the “true” G12 density. The comparison is at uniform grid points within a volume of radius  $40 h^{-1}\text{Mpc}$ . Left: The input to POTENT is the true, G12-smoothed radial velocity. The small scatter of 2.5% reflects small deviations from potential flow, the scatter in the non-linear approximation Eq. 7, and numerical errors. Right: The input is noisy and sparsely-sampled mock data. Shown is the average of 10 random realizations. The global bias is only -4% (Dekel *et al.* 1997).

## 2.7. Maps of Velocity and Density Fields

Figure 4 shows Supergalactic-plane maps of the velocity field in the CMB frame and the associated  $\delta_{c+}$  field (for  $\Omega=1$ ) as recovered by POTENT from the Mark III catalog. The recovery is reliable out to  $\sim 60 h^{-1}\text{Mpc}$  in most directions outside the Galactic plane ( $Y=0$ ). Both large-scale ( $\sim 100 h^{-1}\text{Mpc}$ ) and small-scale ( $\sim 10 h^{-1}\text{Mpc}$ ) features are important; *e.g.*, the bulk velocity reflects properties of the initial fluctuation power spectrum (§ 3), while the small-scale variations indicate the value of  $\Omega$  (§ 4).

The velocity map shows a clear tendency for motion from right to left, in the general direction of the LG motion in the CMB frame ( $L, B = 139^\circ, -31^\circ$  in Supergalactic coordinates). The bulk velocity within  $60 h^{-1}\text{Mpc}$  is  $300 - 350 \text{ km s}^{-1}$  towards ( $L, B \approx 166^\circ, -20^\circ$ ) (§ 3.1) but the flow is not coherent over the whole volume sampled, *e.g.*, there are regions in front of PP (bottom right) and behind the GA (far left) where the  $XY$  velocity components vanish, *i.e.*, the streaming relative to the LG is opposite to the bulk flow direction. The velocity field shows local convergences and divergences which indicate strong density variations on scales about twice as large as the smoothing scale.

The bottom panel of Fig. 4 shows the POTENT mass density field in the Supergalactic plane as a landscape plot. The Great Attractor (with  $12 h^{-1}\text{Mpc}$  smoothing and  $\Omega=1$ ) is a broad density ramp of maximum height  $\delta = 1.4 \pm 0.3$  located near the Galactic plane  $Y=0$  at  $X \approx -40 h^{-1}\text{Mpc}$ . The GA extends towards Virgo near  $Y \approx 10$  (the “Local Supercluster”), towards Pavo-Indus-Telescopium (PIT) across the Galactic plane to the south ( $Y < 0$ ), and

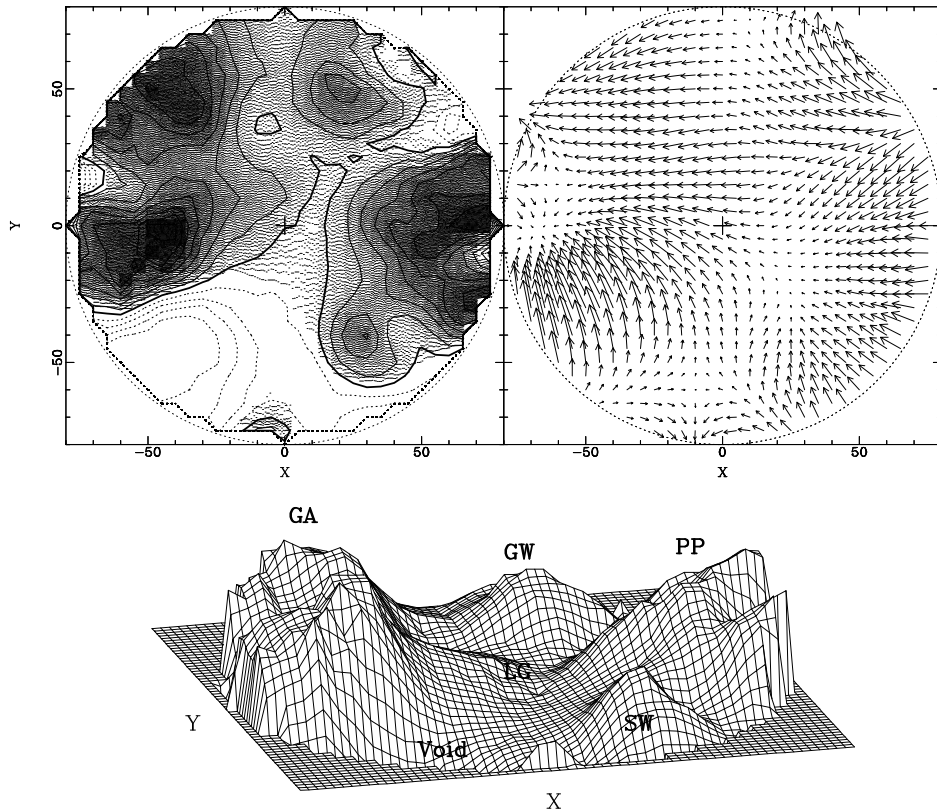


Fig. 4.— POTENT dark-matter maps. The G12 fluctuation fields of peculiar velocity and *mass*-density in the Supergalactic plane as recovered by POTENT from the Mark III peculiar velocities. The vectors are projections of the 3D velocity field in the CMB frame, dominated by large derivatives embedded in a coherent bulk flow. Distances and velocities are in  $100 \text{ km s}^{-1}$ . Contour spacing is 0.2 in  $\delta$ , with the heavy contour marking  $\delta = 0$  and dashed contours  $\delta < 0$ . The height in the surface plot is proportional to the total mass density contrast  $\delta$ . The LG is at the center, GA on the left, PP and the Southern Wall on the right, Coma Great Wall at the top, and the Sculptor void in between (Dekel *et al.* 1997).

towards the Shapley concentration behind the GA ( $Y > 0, X < 0$ ). The structure at the top is related to the “Great Wall” of Coma, with  $\delta \approx 0.6$ . The Perseus Pisces peak which dominates the right-bottom is peaked near Perseus with  $\delta = 1.0 \pm 0.4$ . PP extends towards the southern galactic hemisphere (Aquarius, Cetus), coinciding with the “Southern Wall” as seen in redshift surveys. Underdense regions separate the GA and PP, extending from bottom-left to top-right. The deepest region in the Supergalactic plane, with  $\delta = -0.8 \pm 0.2$ , roughly coincides with the galaxy-void of Sculptor and is useful in bounding  $\Omega$  (§ 4).

### 3. STATISTICS OF MASS-DENSITY FLUCTUATIONS

Having assumed evolution by GI, the structure can be traced backward in time in order to recover the initial fluctuations and to measure statistics which characterize them as a random field, *e.g.*, the power spectrum,  $P(k)$ , and the probability distribution functions (PDF). “Initial” here may refer either to the *linear* regime at  $z \sim 10^3$  after the onset of the self-gravitating matter era, or to the origin of fluctuations in the early universe before being filtered on sub-horizon scales during the plasma-radiation era. The spectrum is filtered on scales  $\leq 100 h^{-1}\text{Mpc}$  by dark-matter dominated processes, but its shape on scales  $\geq 10 h^{-1}\text{Mpc}$  is not affected much by the mildly-nonlinear effects (because the faster density growth in superclusters roughly balances the slower density depletion in voids at the same wavelength). The shape of the one-point PDF, on the other hand, is expected to survive the plasma era unchanged but it develops strong skewness even in the mildly-nonlinear regime. Thus, the present day  $P(k)$  can be used as is to constrain the origin of fluctuations (on large scales) and the nature of the DM (on small scales), while the PDF needs to be traced back to the linear regime first.

The competing scenarios of LSS formation are reviewed for example by Primack (1997). In summary, if the dark matter (DM) is all baryonic, then by nucleosynthesis constraints the universe must be of low density,  $\Omega \lesssim 0.1$ , and a viable model for LSS is the Primordial Isocurvature Baryonic model (PIB) with several free parameters. With  $\Omega \sim 1$ , the non-baryonic DM constituents are either “cold” or “hot”, and the main competing models are CDM, HDM, and CHDM — a 7:3 mixture of the two. The main difference in the DM effect on  $P(k)$  arises from free-streaming damping of the “hot” component of fluctuations on galactic scales. Currently popular variants of the standard CDM model ( $\Omega = 1$ ,  $n = 1$ ) include a tilted power spectrum on large scales ( $n \lesssim 1$ ) and a flat, low- $\Omega$  universe with a non-zero cosmological constant such that  $\Omega + \Omega_\Lambda = 1$ .

The peculiar velocities of the Mark III catalog enable direct derivations of the mass power spectrum itself, independent of galaxy biasing, roughly in the range  $10\text{--}100 h^{-1}\text{Mpc}$ . The bulk velocity in spheres of radii up to  $60 h^{-1}\text{Mpc}$  is sensitive to even larger wavelengths. In all standard theories, the power spectrum on large scales is expected to be a power law,  $P_k \propto k^n$ , with  $n$  of order unity. It is expected to turn around at  $k_{peak} \sim 0.065(\Omega h)^{-1}(h^{-1}\text{Mpc})^{-1}$ , corresponding to the horizon scale at the epoch of equal energy densities in matter and radiation. The dark matter type mostly affects the shape of the filtered spectrum in the “blue” side of the peak ( $k > k_{peak}$ ). Once the fluctuation amplitude on very large-scales is fixed by COBE’s measurements of CMB fluctuations, the bulk velocity is sensitive to  $n$  and is insensitive to  $\Omega$  or the DM type. The steep slope of the CDM-like spectra at  $k > k_{peak}$ , where it is best constrained by the data, makes it more sensitive than the bulk velocity to  $\Omega h$ .

We first describe the bulk velocity (§ 3.1). Then two ways of evaluating  $P(k)$ : a model-independent evaluation from the velocity field via POTENT (§ 3.2), and a likelihood estimation from raw radial peculiar velocities under a prior model (§ 3.3). The  $P(k)$  from the local velocities is then compared to sub-degree angular power spectrum of CMB fluctuations

(§ 3.4).

### 3.1. Bulk Velocity

A simple and robust statistic related to the power spectrum is the bulk velocity — the amplitude of the vector average  $\mathbf{V}$  of the  $R_s$ -smoothed velocity field  $\mathbf{v}(\mathbf{x})$  over a volume defined by a normalized window function  $W_R(\mathbf{r})$  (*e.g.*, top-hat) of a characteristic scale  $R$ ,

$$\mathbf{V} \equiv \int d^3x W_R(\mathbf{x}) \mathbf{v}(\mathbf{x}), \quad \langle V^2 \rangle = \frac{f(\Omega)^2}{2\pi^2} \int_0^\infty dk P(k) \widetilde{W}_R^2(\mathbf{k}). \quad (8)$$

We denote by  $V_r$  the bulk velocity in a top-hat sphere of radius  $R = r h^{-1}\text{Mpc}$ . The ensemble variance  $\langle V^2 \rangle$  for a model that is characterized by  $P(k)$  is an integral of  $P(k)$  in which the wavelengths  $\geq R$  are emphasized by  $\widetilde{W}_R^2(\mathbf{k})$ , the Fourier transform of  $W_R(\mathbf{r})$ . The bulk velocity can be obtained from the observed radial velocities by minimizing residuals as in Eq. 3. The first report by Dressler *et al.* (1987) of  $V = 599 \pm 104$  for ellipticals within  $\sim 60 h^{-1}\text{Mpc}$  was interpreted prematurely as being in severe excess of common predictions, but it quickly became clear that the effective window was much smaller due to the nonuniform sampling and weighting (Kaiser 1988). The sampling-gradient bias can be crudely corrected by volume weighting as in POTENT (§ 2.4), at the expense of larger noise. Courteau *et al.* (1993) reported based on an early version of the Mark III data  $V_{60} = 360 \pm 40$  towards  $(L, B) = (162^\circ, -36^\circ)$ . Alternatively,  $\mathbf{V}_r$  can be computed from the POTENT  $\mathbf{v}$  field by simple vector averaging from the grid.

The bulk velocity as a function of  $R$ , from several recent sources, is shown in Figure 5. The Mark III POTENT result at  $R = 50 h^{-1}\text{Mpc}$  is  $V_{50} = 374 \pm 85 \text{ km s}^{-1}$  towards  $(158^\circ, -9^\circ) \pm 10^\circ$ . The  $\sim 20\%$  error bars are due to distance errors, and one should consider an additional uncertainty of similar magnitude due to the non-uniform sampling. The SFI sample of Sc galaxies yields at the same  $R$  a very similar result (contrary to premature rumors),  $V_{50} \approx 364 \text{ km s}^{-1}$  towards  $(172^\circ, -14^\circ)$  (daCosta *et al.* 1996). These samples are not large enough for a reliable estimate of  $V$  at larger radii.

Supernovae Type Ia provide more accurate distances, with only  $\sim 8\%$  error, and they can be measured at larger distances. The current sample of 44 such SNe by Riess & Kirshner (1997, following Riess, Press & Kirshner 1995), which extends out to  $\sim 300 h^{-1}\text{Mpc}$ , shows a bulk flow of  $V = 253 \pm 252 \text{ km s}^{-1}$  towards  $(166^\circ, -44^\circ)$ . The effective radius of this data set for a bulk flow fit is in fact less than  $50 h^{-1}\text{Mpc}$  because the data is weighted inversely by the errors. The SNe bulk flow is consistent with the results from the Mark III and SFI galaxy data. They all make a bulk of sense within the framework of standard isotropic and homogeneous cosmology.

The only apparently discrepant result comes from the velocities measured on a larger scale using brightest cluster galaxies (BCG) as distance indicators (Lauer & Postman 1994, LP). They indicate a large bulk velocity of  $V = 689 \pm 178$  towards a very different direction  $\sim (126, 21)$ . An ongoing effort to measure BCG's in a larger sample of clusters and distances

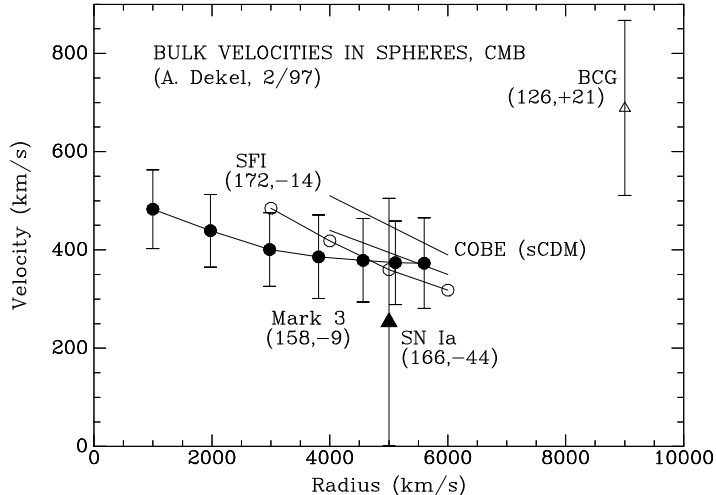


Fig. 5.— Bulk velocity. The amplitude of the bulk velocity relative to the CMB frame in top-hat spheres about the LG, as derived from several data sets. The directions are indicated in supergalactic coordinates  $(L, B)$ . The Mark III data and the SFI data yield consistent results. The new result from Supernovae type Ia on larger scales is a natural extrapolation. The result from brightest galaxies in clusters (LP) is discrepant at more than the  $2 - \sigma$  level.

to clusters based on other distance indicators will soon tell whether this early result is a  $\gtrsim 2\sigma$  statistical fluke (Watkins & Feldman 1995; Strauss *et al.* 1995), whether the errors were underestimated, or whether something is systematically different between the BCG distances and the distances measured by other indicators.

Shown in comparison are the expected *rms* bulk velocity in a standard CDM model ( $\Omega = 1$ ,  $n = 1$ ) normalized to COBE, for  $h = 0.5$  (bottom) and  $0.8$  (top) (Sugiyama 1995). These theoretical curves would not change much if a 20% hot component is mixed with the cold dark matter, or if  $\Omega$  is lower but still in the range  $0.2 - 1.0$ , as long as  $n \approx 1$ . The main effect of  $\Omega$  and  $H_0$  on  $P(k)$  is via  $k_{peak}$ . The predicted bulk velocity over  $\sim 100 h^{-1}\text{Mpc}$  is effectively an integral of  $P(k)$  over  $k < k_{peak}$ , and is therefore relatively insensitive to  $\Omega$  while it is quite sensitive to  $n$ . When compared to a theoretical prediction, the error should also include cosmic scatter due to the fact that only one sphere has been sampled from a random field. These errors are typically on the order of the measurement errors.

The measurements of CMB fluctuations on scales  $\leq 90^\circ$  are independent of the local streaming motions, but GI predicts an intimate relation between their amplitudes. The CMB fluctuations are associated with fluctuations in gravitational potential, velocity and density in the surface of last scattering at  $z \sim 10^3$ , while similar fluctuations in our neighborhood have grown by gravity to produce the dynamical structure observed locally. The comparison between the two is therefore a crucial test for GI.

Before COBE, the local streaming velocities served to predict the expected level of CMB fluctuations. The local surveyed region of  $\sim 100 h^{-1}\text{Mpc}$  corresponds to a  $\sim 1^\circ$  patch on the last-scattering surface. An important effect on scales  $\geq 1^\circ$  is the Sachs-Wolfe effect (1967), where potential fluctuations  $\Delta\Phi_g$  induce temperature fluctuations via gravitational

redshift,  $\delta T/T = \Delta\Phi_g/(3c^2)$ . Since the velocity potential is proportional to  $\Phi_g$  in the linear and mildly-nonlinear regimes,  $\Delta\Phi_g \sim Vx$ , where  $x$  is the scale over which the bulk velocity is  $V$ . Thus  $\delta T/T \geq Vx/(3c^2)$ . A typical bulk velocity of  $\sim 300 \text{ km s}^{-1}$  across  $\sim 100 h^{-1} \text{ Mpc}$  (§ 3.1) corresponds to  $\delta T/T \geq 10^{-5}$  at  $\sim 1^\circ$ . If the fluctuations are roughly scale-invariant ( $n = 1$ ), then  $\delta T/T \geq 10^{-5}$  is expected on all scales  $> 1^\circ$ . Bertschinger, Gorski & Dekel (1990) produced a crude  $\delta T/T$  map of the local region as seen by a hypothetical distant observer, and predicted  $\delta T/T \geq 10^{-5}$  from the local potential well associated with the GA. An up-to-date version of the  $\delta T/T$  maps is provided by Zaroubi *et al.* (1997b), who added a proper treatment of the acoustic effects on sub-degree scales for various cosmological models.

Now that CMB fluctuations of  $\sim 10^{-5}$  have been detected practically on all the relevant angular scales, the argument can be reversed: if one assumes GI, then the *expected* bulk velocity in the surveyed volume is  $\sim 300 \text{ km s}^{-1}$ , *i.e.*, the inferred motions of § 2 are most likely real. If, alternatively, one accepts the peculiar velocities as real for other reasons, then their consistency with the CMB fluctuations is a relatively sensitive and robust test of the validity of GI. This test is unique in the sense that it addresses the specific fluctuation growth rate as predicted by GI theory (§ 5.1). It is robust in the sense that it is quite insensitive to the values of the cosmological parameters and is independent of the complex issues involved in the process of galaxy formation.

### 3.2. Power Spectrum from the Velocity Field via POTENT

One way to compute the power spectrum is via the smoothed mass density field as recovered by POTENT (Kolatt & Dekel 1997). The key is to correct the result for systematic deviations from the true  $P(k)$ . The data suffers from distance errors and sparse, nonuniform sampling, and they were heavily smoothed. The  $P(k)$  is computed from within a window of effective radius  $\sim 50 h^{-1} \text{ Mpc}$ , say, where the densities are weighted inversely by the squares of the local errors. The density field is zero-padded in a larger periodic box in order to enable an FFT procedure. The  $P(k)$  is computed by averaging the amplitudes of the Fourier transforms in bins of  $k$ . This procedure yields an “observed”  $P(k)$ , which we term  $O(k)$ .

The systematic errors in the above procedure are then modeled by  $O(k) = M(k)[S(k) + N(k)]$ , where  $S(k)$  is the true signal  $P(k)$ ,  $N(k)$  is the noise, and  $M(k)$  represents the effects of sampling, smoothing, applying a window etc. The correction functions  $M(k)$  and  $N(k)$  can be derived from Monte Carlo mock catalogs (§ 2.6). The factor  $M(k)$  is derived first by  $M^{-1} = S/\langle O \rangle_{no-noise}$ , where  $S$  here is the known power spectrum built into the simulations, and the averaging is over mock catalogs not perturbed by noise. Then  $N(k)$  is computed by  $N = M^{-1}\langle O \rangle_{noise} - S$ , where the averaging is over noisy mock catalogs.

Equipped with the correction functions  $M(k)$  and  $N(k)$ , the  $P(k)$  observed from the real universe,  $O(k)$ , is corrected to yield the true  $P(k)$  by  $S(k) = M(k)^{-1}O(k) - N(k)$ . The recovered mass-density  $P(k)$  is shown in Figure 6 in three thick logarithmic bins covering the range  $0.04 \leq k \leq 0.2 (h^{-1} \text{ Mpc})^{-1}$ , within which the results are reliable. The robust result is  $P(k)f(\Omega)^2 = (4.6 \pm 1.4) \times 10^3 (h^{-1} \text{ Mpc})^3$  at  $k = 0.1 (h^{-1} \text{ Mpc})^{-1}$  (using the convention where

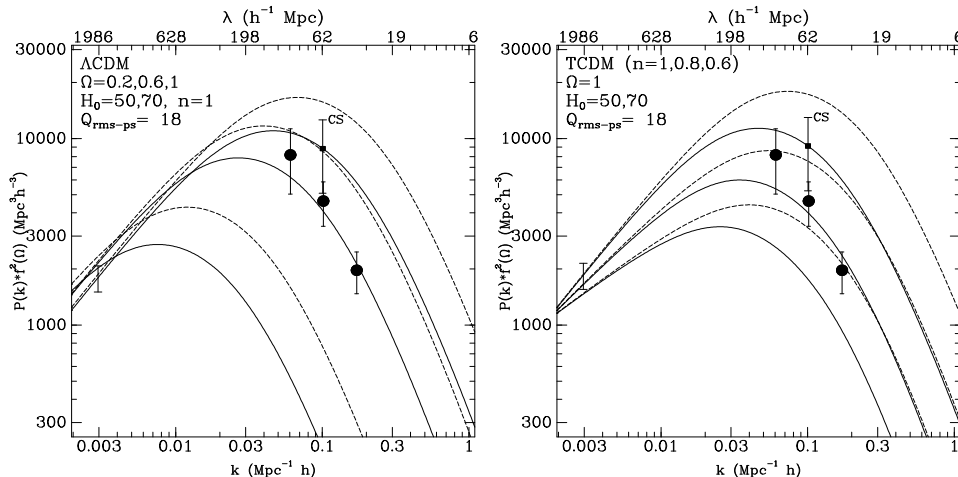


Fig. 6.— The mass power spectrum  $[\times f(\Omega)^2]$  from POTENT Mark III velocities (filled symbols), with  $1\sigma$  random errors. The curves are COBE-normalized theoretical predictions for flat CDM with  $h = 0.5$  (solid) and  $h = 0.7$  (dashed). Left:  $\Lambda$ -CDM with  $n = 1$  and  $\Omega$  growing upwards. Right: tilted-CDM with  $\Omega = 1$  and  $n$  growing upwards. Typical cosmic scatter (CS) for  $\Omega = 1$  and  $n = 1$  is indicated (Kolatt & Dekel 1997).

the Fourier transform is defined with no  $2\pi$  factors in it's coefficient). The logarithmic slope at  $k = 0.1$  is  $-1.45 \pm 0.5$ . This translates to  $\sigma_8 \Omega^{0.6} \simeq 0.7 - 0.8$ , depending on where the peak in  $P(k)$  is (see § 3.3).

The observed  $P(k)$  is compared in the figure to the linear predictions of a family of Inflation-motivated flat CDM models ( $\Omega + \Omega_\Lambda = 1$ ), normalized by the 4-year COBE data, with the Hubble constant fixed at  $h = 0.5$  or  $h = 0.7$ . For  $n = 1$ , maximum likelihood is obtained at  $\Omega \simeq 0.7h_{50}^{-1.3} \pm 0.1$ . For  $\Omega = 1$ , assuming no tensor fluctuations, the linear power index is  $n \simeq 0.75h_{50}^{-0.8} \pm 0.1$ .

### 3.3. Power Spectrum from Velocities for COBE-CDM Models

The power spectrum, in a parametric form including  $\Omega$ ,  $h$  and  $n$  among the parameters, has alternatively been determined from the velocity data via a Bayesian likelihood analysis (Zaroubi *et al.* 1997a; see also Kaiser & Jaffe 1995). According to Bayse, the probability of the model parameters ( $m$ ) given the data ( $d$ ), which is the function one wishes to maximize, can be expressed as  $P(m|d) = P(d|m)P(m)/P(d)$ . The probability  $P(d)$  serves here as a normalization constant. Without any external constraints on the model parameters, one assumes that  $P(m)$  is a constant in a given range. The remaining task is to maximize the likelihood  $\mathcal{L} = P(d|m)$  as a function of the model parameters. This function can be written down explicitly.

Under the assumption that the velocities and the errors are both Gaussian random fields with no mutual correlations, the likelihood can be written as  $\mathcal{L} = (2\pi|D|)^{-1/2} \exp(-d_i D_{ij}^{-1} d_j/2)$ ,



where  $d_i$  are the data at points  $i = 1, \dots, N$ , and  $D_{ij}$  is the covariance matrix, which can be split into covariance of signal ( $s$ ) and covariance of noise ( $n$ ),  $D_{ij} \equiv \langle d_i d_j \rangle = \langle s_i s_j \rangle + \langle n_i n_j \rangle$ . If the errors are uncorrelated, the noise matrix is diagonal. The signal matrix is computed from the model  $P(k)$  as a function of the model parameters.

Zaroubi *et al.* (1997a) used a parametric model for the PS of the general form  $P_k = A k^n T(\Gamma_i; k)$ , where  $T(k)$  is a small-scale filter of an assumed shape characterized by free parameters  $\Gamma_i$ ,  $k^n$  is the initial  $P(k)$  which is still valid on large scales today, and  $A$  is a normalization factor. The normalization can either be determined by COBE's data (for given  $\Omega$ ,  $\Lambda$ ,  $h$ ,  $n$  and tensor/scalar fluctuations), or be left as a free parameter to be fixed by the velocity data alone. The filter  $T(k)$  can either be taken from a specific physical model (*e.g.*, CDM, where  $\Gamma = \Omega h$ ), or be an arbitrary function with enough flexibility to fit the data.

The robust result for all the models is a relatively high amplitude, with  $P(k)f(\Omega)^2 = (4.8 \pm 1.5) \times 10^3 (h^{-1}\text{Mpc})^3$  at  $k = 0.1 (h^{-1}\text{Mpc})^{-1}$ . An extrapolation to smaller scales using the different CDM models yields  $\sigma_8 \Omega^{0.6} = 0.88 \pm 0.15$  (for the dispersion in top-hat spheres of radius  $8 h^{-1}\text{Mpc}$ ).

Within the general family of CDM models, allowing for a cosmological constant in a flat universe and a tilt in the spectrum, the parameters are confined by a 90% likelihood contour of the sort  $\Omega h_{50}^\mu n^\nu = 0.8 \pm 0.2$ , where  $\mu = 1.3$  and  $\nu = 3.4, 2.0$  for models with and without tensor fluctuations respectively. Figure 7 displays the likelihood map in the  $\Omega - n$  plane for these models. For open CDM the powers are  $\mu = 0.95$  and  $\nu = 1.4$  (no tensor fluctuations). A  $\Gamma$ -shape model free of COBE normalization yields only a weak constraint:  $\Gamma = 0.4 \pm 0.2$  (where  $\Gamma$  is not necessarily  $\Omega h$ ).

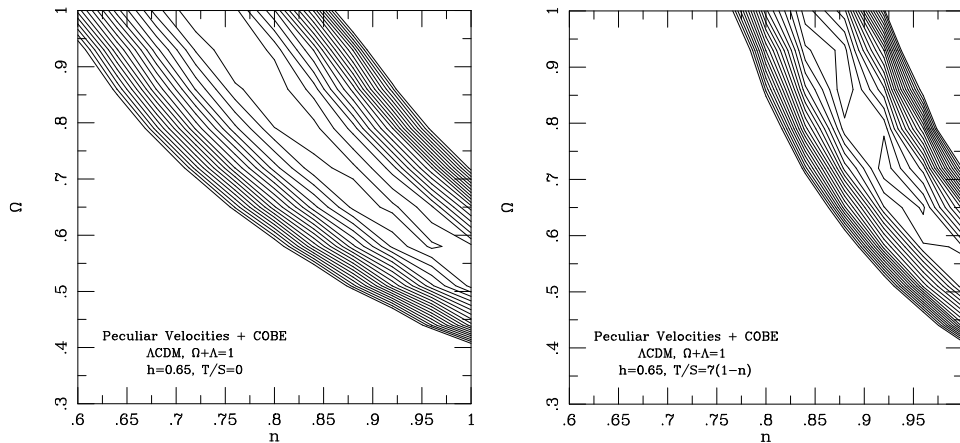


Fig. 7.— Likelihood contour maps in the  $\Omega - n$  plane for flat CDM with and without tensor fluctuations and  $h = 0.65$ . Contour spacing is unity in log-likelihood. Under the assumption of a  $\chi^2$  distribution, the two-dimensional 90 percentile corresponds to 2.3 contours, and the one-dimensional 90 percentile corresponds to 1.35 contours (Zaroubi *et al.* 1997a).

Both  $\Omega$  and  $n$  obtained by the likelihood analysis from the raw peculiar velocities tend

to be slightly higher ( $\sim 20\%$ ) than their estimates based on the  $P(k)$  recovered from the POTENT output. This difference may arise from the different relative weighting assigned to the different wavelengths in the two analyses. The difference between the results obtained in the two different ways is on the order of the errors in each analysis and the cosmic scatter. Very similar estimates of  $P(k)$  are obtained from a preliminary analysis of the SFI sample of Sc galaxies (in preparation).

In summary: The “standard” CDM model is marginally rejected at the  $\sim 2\sigma$  level, while each of the following modifications lead to a good fit to the peculiar velocities and large-scale CMB data:  $n \lesssim 1$ ,  $\Omega_\nu \sim 0.3$ , or  $\Omega \lesssim 1$ . The strong implication on the dark matter issue is that values of  $\Omega$  as low as  $\sim 0.2$  are ruled out with high confidence (independent of  $\Lambda$ ), leaving, in particular, no room for the baryonic PIB model.

### 3.4. Peculiar Velocities vs Small-scale CMB Fluctuations

Sub-degree angular scales at the last scattering surface correspond to the  $\leq 100 h^{-1}\text{Mpc}$  comoving scales explored by peculiar velocities today. Thus, under the assumption that the local neighborhood is typical, the power spectrum on these scales is simultaneously constrained by the mass-density fluctuations in our cosmological neighborhood and by the CMB fluctuations.

The sub-degree CMB fluctuations are now being explored by many balloon-born experiments, and in less than a decade we expect accurate results from the CMB satellites MAP and Planck. These measurements will eventually allow a simultaneous likelihood analysis of the two kinds of data. At this point, however, although there are already preliminary detections of the first acoustic peak in the angular power spectrum, the uncertainties are still large. Any current comparison is therefore limited to the semi-quantitative level. The range of parameters permitted by the peculiar velocity data for power spectra of the CDM family (Zaroubi *et al.* 1997a) can be translated to a range of angular power spectra,  $C_l$ . This range is plotted against current observations in Figure 8.

The immediate conclusions from a visual inspection of the figure are that a wide range of CDM models can simultaneously obey the two data sets, but there is a subset of models that fits the velocities well but seems to fail to produce a high enough acoustic peak in the CMB spectrum.

The acoustic peak in the CMB is sensitive to  $\Omega_b$  and the observations prefer a high baryon content,  $\Omega_b h^2 \sim 0.025$  (similar to the value measured by Tytler *et al.* 1996; Burles & Tytler 1996), while the peculiar velocities have little to add because  $P(k)$  is hardly affected by  $\Omega_b$ .

The power index  $n$  is important in both cases; the peculiar velocities allow values of  $n$  significantly lower than unity, but the current CMB data seem not to tolerate values of  $n$  below 0.9 or so.

The peculiar velocity data prefers  $\Omega \geq 0.4$ , and the location of the first acoustic peak

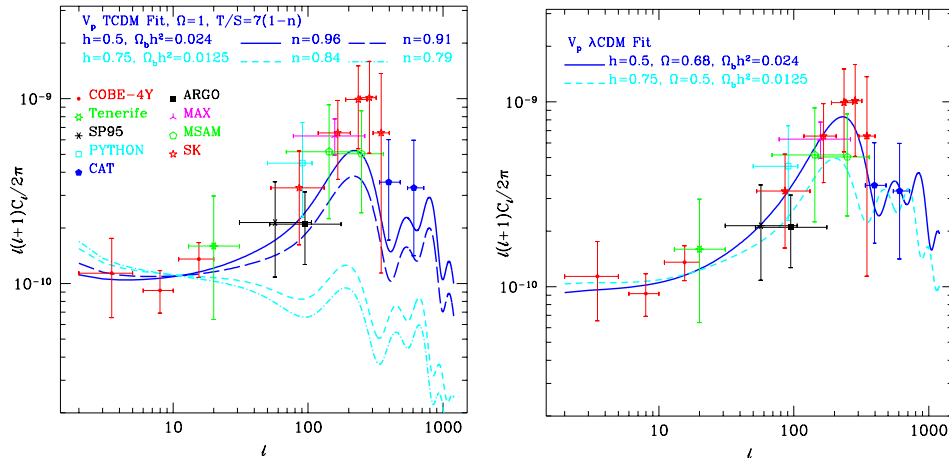


Fig. 8.— Angular power spectrum in the CMB. The current data (symbols) are compared to certain CDM models that fit the peculiar velocity data at 90% likelihood. The extreme models shown are either with low  $h$  and high  $\Omega_b h^2$  or vice versa. Left: tilted CDM with  $\Omega = 1$ , including tensor fluctuations. Right: Flat CDM with  $n = 1$  (Zaroubi *et al.* 1997b). xxxxxxx

in the sub-degree CMB data indicates in agreement a high value of  $\Omega + \Omega_\Lambda$ .

#### 4. DIRECT MEASUREMENTS OF $\Omega$ FROM PECULIAR VELOCITIES

Assuming that the inferred motions are real and generated by GI, they can be used to estimate  $\Omega$  in several different ways. Most of the evidence from virialized systems on scales  $\leq 10 h^{-1}\text{Mpc}$  suggest a low mean density of  $\Omega \sim 0.2$  (see Dekel, Burstein & White 1997). The spatial *variations* of the large-scale velocity field provide ways to measure the mass density in a larger volume that may be closer to a “fair” sample. One family of such methods is based on comparing the dynamical fields derived from velocities to the fields derived from galaxy redshifts (§ 5). These methods can be applied in the linear regime but they always rely on the assumed biasing relation between galaxies and mass often parameterized by  $b$ , so they actually provide an estimate of  $\beta \equiv f(\Omega)/b$ . Another family of methods measures  $\beta$  from redshift surveys alone, based on  $z$ -space deviations from isotropy (see Strauss 1997). In the present section, we focus first on methods that rely on non-linear effects in the peculiar velocity data *alone*, and they thus provide estimates of  $\Omega$  independent of galaxy density biasing. These methods are based on the assumption that the initial fluctuations were Gaussian.

##### 4.1. Divergence in Voids

A diverging flow in an extended low-density region can provide a robust dynamical lower bound on  $\Omega$ , based on the fact that large gravitating outflows are *not* expected in a low- $\Omega$

universe (Dekel & Rees 1994). In practice, for any assumed value of  $\Omega$ , the partial derivatives of the smoothed observed velocity field are used to infer a non-linear approximation for the mass density via the approximation  $\delta_c$  (6). A key point is that this approximation is typically an overestimate,  $\delta_c > \delta$  (when the true value of  $\Omega$  is used). For fluctuations that started Gaussian, the probability that  $\delta_c$  is an overestimate, in the range  $\delta < -0.5$ , is well over 99%. Analogously to  $\delta_0 \approx -\Omega^{-0.6} \nabla \cdot \mathbf{v}$ , the  $\delta_c$  inferred from a given diverging velocity field is more negative when a smaller  $\Omega$  is assumed, so for a small enough  $\Omega$  one may obtain  $\delta < -1$  in certain void regions. Such values of  $\delta$  are forbidden because mass is never negative, so this provides a lower bound on  $\Omega$ .

The inferred  $\delta_c$  field, smoothed at  $12 h^{-1} \text{Mpc}$ , and the associated error field  $\sigma_\delta$ , were derived by POTENT at grid points from the observed radial velocities of Mark III. Focusing on the deepest density wells, the input  $\Omega$  was lowered until  $\delta_c$  became significantly smaller than  $-1$ . The most promising “test case” provided by the Mark III data is a broad diverging region centered near the supergalactic plane at the vicinity of  $(X, Y) = (-25, -40)$  in  $h^{-1} \text{Mpc}$  — the “Sculptor void” of galaxies between the GA and the “Southern Wall” extension of PP (Figure 9, compare to Fig. 4).

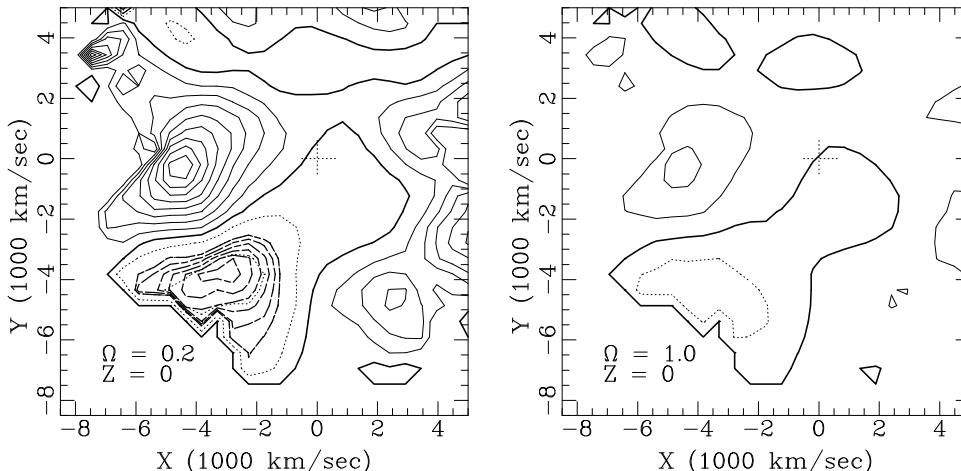


Fig. 9.— Maps of  $\delta_c$  inferred from the observed velocities near the Sculptor void in the Supergalactic plane, for two values of  $\Omega$ . The LG is marked by ‘+’ and the void is confined by the Pavo part of the GA (left) and the Aquarius extension of PP (right). Contour spacing is 0.5, with  $\delta_c = 0$  heavy,  $\delta_c > 0$  solid, and  $\delta_c < 0$  dotted. The heavy-dashed contours mark the illegitimate downward deviation of  $\delta_c$  below  $-1$  in units of  $\sigma_\delta$ , starting from zero (*i.e.*,  $\delta_c = -1$ ) and decreasing with spacing  $-0.5\sigma_\delta$ . The value  $\Omega = 0.2$  is ruled out at the  $2.9\sigma$  level (Dekel & Rees 1994).

Values of  $\Omega \approx 1$  are perfectly consistent with the data, but  $\delta_c$  becomes smaller than  $-1$  already for  $\Omega = 0.6$ . The values  $\Omega = 0.3$  and  $0.2$  are ruled out at the  $2.4\sigma$  and  $2.9\sigma$  levels in terms of the random error  $\sigma_\delta$ .

This result is still to be improved. The systematic errors have been partially corrected in POTENT, but a more specific investigation of the biases affecting the smoothed velocity field in density wells is still in progress. For the method to be effective one needs to find a void that is (a) bigger than the correlation length for its vicinity to represent the universal

$\Omega$ , (b) deep enough for the lower bound to be tight, (c) nearby enough for the distance errors to be small, and (d) properly sampled to trace the velocity field in its vicinity.

Note that this method does not require that the void be spherical or of any other particular shape, and is independent of galaxy density biasing. Another pro is that there is no much cosmic scatter — one deep and properly sampled void is enough for a meaningful constraint. The main limitation is the poor (and perhaps biased) sampling of the velocity field in the vicinity of a void.

## 4.2. Deviations from Gaussian PDF

Assuming that the initial fluctuations are a Gaussian random field, the one-point probability distribution function (PDF) of smoothed density develops a characteristic skewness due to non-linear effects early in the non-linear regime (*e.g.*, Kofman *et al.* 1994). The skewness of  $\delta$  is given according to second-order perturbation theory by

$$\langle \delta^3 \rangle / \langle \delta^2 \rangle^2 \approx (34/7 - 3 - n) , \quad (9)$$

with  $n$  the effective power index of the power spectrum near the (top-hat) smoothing scale (Bouchet *et al.* 1992). Since this ratio of moments for  $\delta$  is practically independent of  $\Omega$ , and since  $\nabla \cdot \mathbf{v} \sim -f\delta$ , the corresponding ratio for  $\nabla \cdot \mathbf{v}$  must strongly depend on  $\Omega$ , and indeed in second-order it is (Bernardeau *et al.* 1995)

$$T_3 \equiv \langle (\nabla \cdot \mathbf{v})^3 \rangle / \langle (\nabla \cdot \mathbf{v})^2 \rangle^2 \approx -f(\Omega)^{-1}(26/7 - 3 - n) . \quad (10)$$

Using N-body simulations and  $12 h^{-1} \text{Mpc}$  smoothing one indeed finds  $T_3 = -1.8 \pm 0.7$  for  $\Omega = 1$  and  $T_3 = -4.1 \pm 1.3$  for  $\Omega = 0.3$ , where the error is the cosmic scatter for a sphere of radius  $40 h^{-1} \text{Mpc}$  in a CDM universe ( $H_0 = 75$ ,  $b = 1$ ). An estimate of  $T_3$  in the current POTENT velocity field within  $40 h^{-1} \text{Mpc}$  is  $-1.1 \pm 0.8$ , where the errors this time represent distance errors. With the two errors added in quadrature,  $\Omega = 0.3$  is rejected at the  $\sim 2\sigma$  level (somewhat sensitive to the assumed  $P(k)$ ).

Since the present PDF contains only part of the information stored in the data and is in some cases not that sensitive to the initial PDF (IPDF), a more powerful bound can be obtained by using the detailed present velocity field  $\mathbf{v}(\mathbf{x})$  to recover the IPDF, and using the latter to constrain  $\Omega$  by measuring its  $\Omega$ -dependent deviation from the assumed normal distribution (Nusser & Dekel 1993). The necessary “time machine” is provided by the Eulerian interpretation of the Zel’dovich approximation (Nusser & Dekel 1992).

The velocity out of POTENT Mark II, within a conservatively selected volume, was fed into the IPDF recovery procedure with  $\Omega$  either 1 or 0.3, and the errors due to distance errors and cosmic scatter were estimated. Figure 10 shows the recovered IPDF’s. The IPDF recovered for  $\Omega = 1$  is marginally consistent with Gaussian, while the one recovered for  $\Omega = 0.3$  shows significant deviations. The largest deviation, bin by bin in the IPDF, is  $\lesssim 2\sigma$  for  $\Omega = 1$  and  $> 4\sigma$  for  $\Omega = 0.3$ , and a similar rejection of  $\Omega = 0.3$  is obtained with a  $\chi^2$ -type

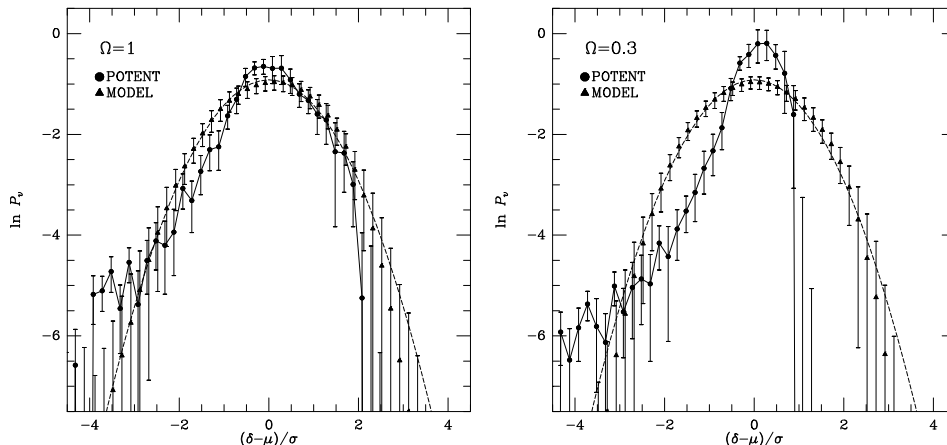


Fig. 10.—  $\Omega$  from IPDF. The density IPDF recovered from the G2 POTENT peculiar velocity field (solid), compared to a normal distribution (short dash) and with the IPDF recovered from the velocity field of Gaussian CDM simulations (triangles). The assumed  $\Omega$  is 1.0 (left) or 0.3 (right). The simulations are of  $\Omega_0 = \Omega$  accordingly (Nusser & Dekel 1993).

statistic. The skewness and kurtosis are poorly determined because of noisy tails but the replacements  $\langle x|x| \rangle$  and  $\langle |x| \rangle$  allow a rejection of  $\Omega = 0.3$  at the  $(5 - 6)\sigma$  levels.

The main advantage of the methods based on the PDF is their insensitivity to galaxy density biasing. The main weakness is the need for a “fair” sample; the cosmic scatter is large due to the large smoothing scale within the limited volume.

## 5. GALAXY DENSITY VS. VELOCITIES: $\Omega$ AND BIASING

### 5.1. Galaxies vs Mass: Fit of GI and Linear Biasing Model

The theory of GI combined with the assumption of linear biasing for galaxies predict a correlation between the dynamical density field and the galaxy density field, which can be addressed quantitatively based on the mock catalogs and the estimated errors in the two data sets. Figure 11 compares density maps in the Supergalactic plane for IRAS 1.2 Jy galaxies ( $\delta_G$ ) and POTENT Mark III mass ( $\delta$ ), both G12 smoothed. The general correlation is evident — the GA, PP, Coma and the voids all exist both as dynamical entities and as structures of galaxies. To evaluate goodness of fit, Figure 12 shows the statistic  $\chi^2 = N^{-1} \sum^N (\delta_G - b\delta)^2 / \sigma^2$  as computed from the data in comparison with its distribution over pairs of Mark III and IRAS 1.2 Jy mock catalogs. The fact that the data lies near the center of this distribution indicates that the two data sets are consistent with being noisy versions of an underlying fluctuation field and that the data are in agreement with the hypotheses of GI plus linear biasing (Dekel *et al.* 1993; Sigad *et al.* 1997; more in § 5.2).

What is it exactly that one can learn from the observed  $\mathbf{v} - \delta_G$  correlation (Babul *et*

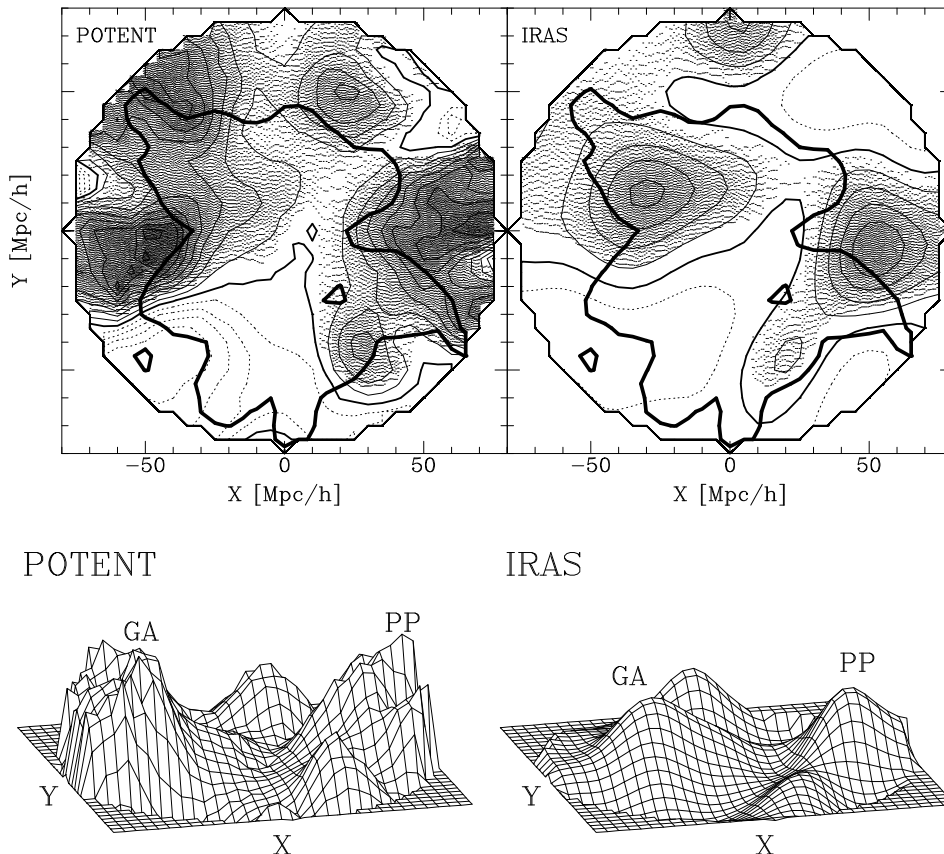


Fig. 11.— Mass versus galaxies. POTENT mass ( $\Omega = 1$ ) versus IRAS galaxy density fields in the Supergalactic plane, both smoothed G12. Contour spacing is 0.2. The heavy contour marks the boundary of the comparison volume of effective radius  $46 h^{-1} \text{Mpc}$ . The height in the surface plot is proportional to  $\delta$ . The LG is at the center, GA on the left, PP on the right, and the Sculptor void in between (Sigad *et al.* 1997).

*al.* 1994)? First, it argues that the velocities are real because it is hard to invoke any other reasonable way to make the galaxy distribution and the TF measurements agree so well. On the other hand, although it is true that gravity is the only long-range force that could attract galaxies to stream toward density concentrations, the fact that a  $\mathbf{v} - \delta_G$  correlation is predicted by GI plus linear biasing does not necessarily mean that the observation can serve as a sensitive test for either. Recall that converging (or diverging) flows tend to generate overdensities (or underdensities) simply as a result of mass conservation, independent of the source of the motions.

Let us assume for a moment that galaxies trace mass, *i.e.*, that the linearized continuity equation,  $\dot{\delta} = -\nabla \cdot \mathbf{v}$ , is valid for the galaxies as well. The observed correlation (in the linear approximation) is then  $\delta \propto -\nabla \cdot \mathbf{v}$ , and together they imply that  $\dot{\delta} \propto \delta$ , or equivalently that  $\nabla \cdot \mathbf{v}$  is proportional to its time average. This property is not exclusive to GI; one can construct counterexamples where the velocities are produced by a non-GI impulse.

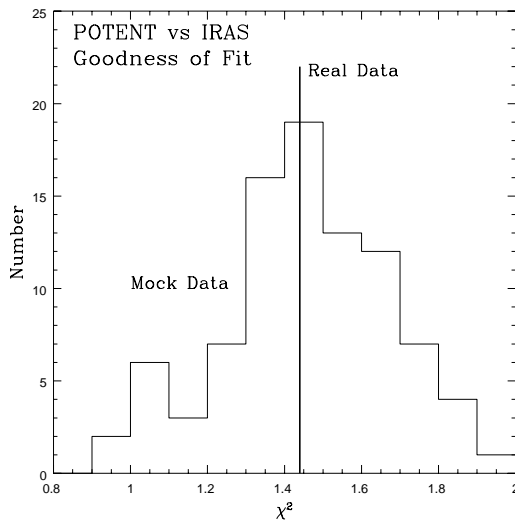


Fig. 12.— Goodness of fit in the comparison of G12 density fields of POTENT mass and IRAS galaxies, as tested by a  $\chi^2$  statistic that is an error weighted sum of differences between the two fields (Sigad *et al.* 1997).

Even irrotationality does not follow from  $\delta \propto -\nabla \cdot \mathbf{v}$ ; it has to be adopted based on theoretical arguments in order to enable reconstruction from radial velocities or from observed densities. Once continuity and irrotationality are assumed, the observed  $\delta \propto -\nabla \cdot \mathbf{v}$  implies a system of equations which is identical in all its *spatial* properties to the equations of GI, but can differ in the constants of proportionality and their temporal behavior. It is therefore impossible to distinguish between GI and a non-GI model which obeys continuity plus irrotationality based only on snapshots of *present-day* linear fluctuation fields. This makes the relation between CMB fluctuations and velocities an especially important test for GI.

On the other hand, the fact that the constant of proportionality in  $\delta \propto -\nabla \cdot \mathbf{v}$  is indeed the same everywhere is a non-trivial requirement from a non-GI model. For example, a version of the explosion scenario (Ostriker & Cowie 1981; Ikeuchi 1981), which tested successfully both for irrotationality and  $\mathbf{v} - \delta$  correlation, requires special synchronization among the explosions (Babul *et al.* 1994).

So, what is the  $\mathbf{v} - \delta_G$  relation good for? While it’s sensitivity to GI is only partial, this relation turns out to be quite sensitive to the validity of a *continuity*-like relation for the *galaxies*. When the latter is strongly violated all bets are off for the  $\mathbf{v} - \delta_G$  relation. A non-linear biasing scheme would make continuity invalid for the galaxies, which would ruin the  $\mathbf{v} - \delta_G$  relation even if GI is valid. The observed correlation is thus a sensitive test for density *biasing*. It implies, subject to the errors, that the  $\sim 12 h^{-1} \text{Mpc}$ -smoothed density fields of galaxies and mass are related via a biasing relation that could be crudely approximated by a linear relation with  $b$  of order unity (but see a refinement of this in § 5.5).

Now that the data of peculiar velocities and the data of galaxy density are found to be compatible with the model of GI and linear biasing, they can be combined to constrain the



degenerate parameter  $\beta \equiv \Omega^{0.6}/b$ . The comparison between the two data sets can be done in several different ways. In particular, it could be done by comparing density fields derived locally from the two data sets (§ 5.2), or by comparing velocities derived from the two data sets (§ 5.4). It can be done successively by first recovering fields from each data set and then combining them to obtain  $\beta$ , or by a simultaneous recovery of fields and beta determination from the two data sets (§ 5.3). It can be done by direct comparison of fields in r-space, or by comparing coefficients mode by mode in a model expansion in z-space (Davis, Nusser & Willick 1996).

## 5.2. Density-Density Comparison on Large Scales: POTIRAS

The main advantage of comparing densities is that they are *local*. The densities are independent of long-range effects due to the unknown mass distribution outside the sampled volume, which could affect the velocities. The densities are also independent of reference frame, and can be reasonably corrected for non-linear effects.

The POTENT analysis extracts from the peculiar velocity data a mildly-nonlinear mass density fluctuation field in a spatial grid, smoothed G12 (§ 2.5). The associated real-space density field of galaxies can be extracted with similar smoothing from a whole-sky redshift survey such as the IRAS 1.2 Jy survey (see Strauss & Willick 1995; Sigad *et al.* 1997).

A brief summary of the recovery of the IRAS density field is as follows. The solution to the linearized GI equation  $\nabla \cdot \mathbf{v} = -f\delta$  for an irrotational field is

$$\mathbf{v}(\mathbf{x}) = \frac{f}{4\pi} \int_{\text{all space}} d^3x' \delta(\mathbf{x}') \frac{\mathbf{x}' - \mathbf{x}}{|\mathbf{x}' - \mathbf{x}|^3}. \quad (11)$$

The velocity is proportional to the gravitational acceleration, which ideally requires full knowledge of the distribution of mass in space. In practice, one is provided with a flux-limited, discrete redshift survey, obeying some radial selection function  $\phi(r)$ . The galaxy density is estimated by  $1 + \delta_G(\mathbf{x}) = \sum n^{-1} \phi(r_i)^{-1} \delta_{dirac}^3(\mathbf{x} - \mathbf{x}_i)$ , where  $n \equiv V^{-1} \sum \phi(r_i)^{-1}$  is the mean galaxy density, and the inverse weighting by  $\phi$  restores the equal-volume weighting. Eq. 11 is then replaced by

$$\mathbf{v}(\mathbf{x}) = \frac{\beta}{4\pi} \int_{r < R_{max}} d^3x' \delta_G(\mathbf{x}') S(|\mathbf{x}' - \mathbf{x}|) \frac{\mathbf{x}' - \mathbf{x}}{|\mathbf{x}' - \mathbf{x}|^3}. \quad (12)$$

Under the assumption of linear biasing, the cosmological dependence enters through  $\beta$ . The integration is limited to  $r < R_{max}$  where the signal dominates over shot-noise.  $S(\mathbf{y})$  is a small-scale smoothing window ( $\geq 500 \text{ km s}^{-1}$ ) essential for reducing the effects of non-linear gravity, shot-noise, distance uncertainty, and triple-value zones.

The distances are estimated from the redshifts in the LG frame by

$$r_i = z_i - \hat{\mathbf{x}}_i \cdot [\mathbf{v}(\mathbf{x}_i) - \mathbf{v}(0)]. \quad (13)$$

Equations 12-13 can be solved iteratively: make a first guess for the  $\mathbf{x}_i$ , compute the  $\mathbf{v}_i$  by Eq. 12, correct the  $\mathbf{x}_i$  by Eq. 13, and so on until convergence. The convergence can be improved by increasing  $\beta$  gradually during the iterations from zero to its desired value.

Even under  $12 h^{-1}\text{Mpc}$  smoothing,  $\delta_G$  is of order unity in places, necessitating a mildly-nonlinear treatment. Local approximations from  $\mathbf{v}$  to  $\delta$  were discussed in § 2.5, but the non-local nature of the inverse problem makes it less straightforward. A possible solution is to find an inverse relation of the sort  $\nabla \cdot \mathbf{v} = F(\Omega, \delta_G)$ , including non-linear gravity and non-linear biasing. This is a Poisson-like equation in which  $-\beta\delta_G(\mathbf{x})$  is replaced by  $F(\mathbf{x})$ , and since the smoothed velocity field is still irrotational for mildly-nonlinear perturbations, it can be integrated analogously to Eq. 11. With smoothing of  $10 h^{-1}\text{Mpc}$  and  $\beta = 1$ , the approximation based on an empirical inverse to  $\delta_c$  (6) has an *rms* error  $< 50 \text{ km s}^{-1}$ .

In recent applications, the galaxy density field is recovered from the noisy IRAS data via a Power-Preserving Filter (PPF, by A. Yahil, described in Sigad *et al.* 1997) — a modification of the Wiener Filter. The PPF returns a field that is not far from the Wiener, most probable field, but it makes the result more realistic by forcing the variance to be constant in space despite the fact that the errors vary.

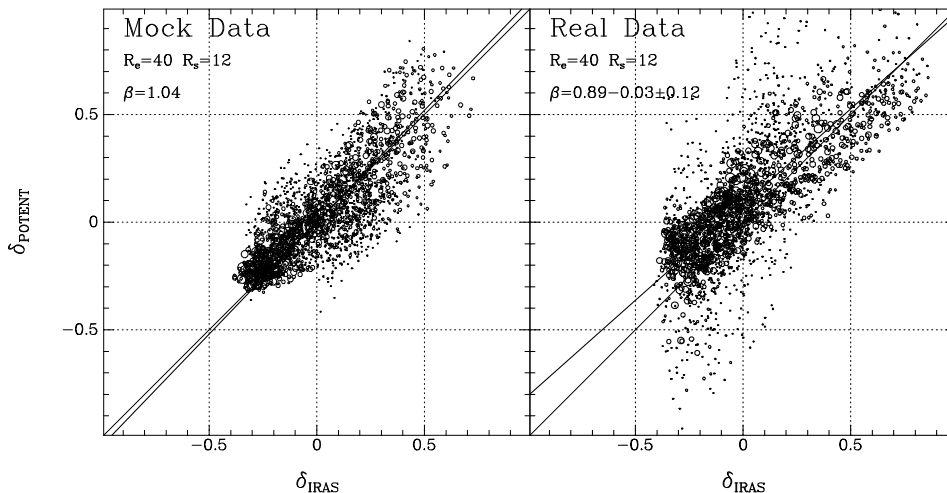


Fig. 13.—  $\beta$  from POTENT vs IRAS density comparison. The smoothing is G12 and the comparison volume is of effective radius  $40 h^{-1}\text{Mpc}$ . Two-dimensional regression lines are marked. Left: Regression between the averages of 20 mock catalogs of each type, showing a bias as small as 4%. Right: Real data (Sigad *et al.* 1997).

The simplest way of comparing the POTENT and IRAS density fields is via a two-dimensional linear regression using the values of the fields at grid points within a local comparison volume. The errors of both fields enter the regression. The comparison volume is determined by equal-error contours.

The latest comparison of POTENT Mark III and IRAS 1.2 Jy data at  $12 h^{-1}\text{Mpc}$  smoothing within a volume of  $(65 h^{-1}\text{Mpc})^3$  yields  $\beta_I = 0.86 \pm 0.12$  (Sigad *et al.* 1997). The corresponding scatter diagram is shown in Figure 13. The systematic error in this derivation,

of only 4%, is deduced from the analogous scatter diagram for the averages of 20 random mock catalogs of each type. This is an update of the higher estimate  $\beta_I = 1.3 \pm 0.3$  (Dekel *et al.* 1993) obtained based on an earlier version of POTENT with the Mark II velocities and the IRAS 1.9 Jy redshifts.

Similar comparisons of the mass density field with the density of optical galaxies indicate a similar correlation and a  $\sim 30\%$  lower estimate for  $\beta_O$  (Hudson *et al.* 1995), in agreement with the ratio of biasing factors,  $b_O/b_I \approx 1.3$ , obtained by direct comparison of optical and IRAS galaxy densities.

A comparison of similar nature of the POTENT Mark III data with the density distribution of Abell/ACO  $R \geq 0$  clusters and the corresponding predicted velocities at G15 smoothing yields similar consistency out to distances of  $\sim 60 h^{-1}\text{Mpc}$ , and an estimate of  $\beta_C = 0.26 \pm 0.11$  (Plionis *et al.* 1997). This is consistent with a linear biasing factor for the clusters that is about 4 times larger than that of galaxies, in accordance with the observed ratio of about  $4^2$  for the corresponding correlation functions (see Bahcall 1997).

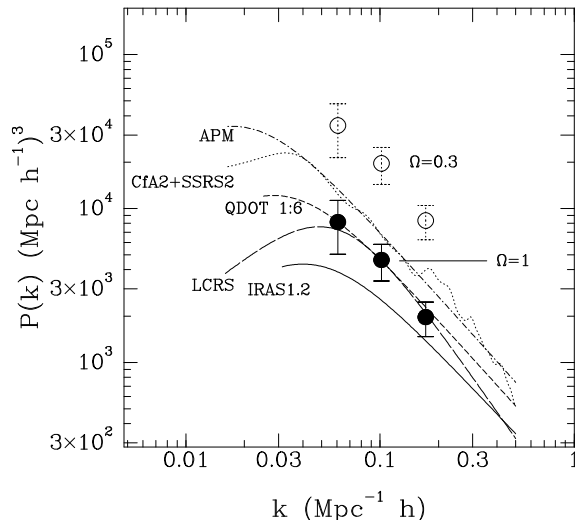


Fig. 14.—  $\beta$  from power spectra of galaxies versus mass. The estimates from various galaxy density samples were all translated from redshift to real space using Kaiser’s approximation and the best-fit value of  $\beta$ . The  $P(k)$  from peculiar velocities (Fig. 6) is marked by solid symbols for  $\Omega = 1$  (open symbols for  $\Omega = 0.3$ ). The values of  $\beta$  (for any  $\Omega$ ) can be read directly from the vertical offset of the solid symbols and the corresponding curves (Kolatt & Dekel 1997).

A direct comparison of the mass power spectrum as derived from peculiar velocities (§ 3.2) with the galaxy power spectra as derived from different redshift and angular surveys is shown in Figure 14 (Kolatt & Dekel 1997). It demonstrates a similarity in shape and yields for the various galaxy types  $\beta$  values in the range  $0.77 - 1.21$ , with a typical error of  $\pm 0.1$ . For IRAS galaxies typically  $\beta \gtrsim 1$ , and for optical galaxies  $\beta \lesssim 1$ . These estimates do not directly address the value of  $\Omega$ , but it is clear from the figure that if  $\Omega$  is as small as  $\sim 0.3$ , then all galaxy types must be severely antibiased.

In principle, the degeneracy of  $\Omega$  and  $b$  is broken in the mildly-nonlinear regime, where

$\delta(\mathbf{v})$  is no longer  $\propto f^{-1}$ . Compatible mildly-nonlinear corrections in POTENT and in the IRAS analysis allowed a preliminary attempt to separate these parameters using the Mark II and IRAS 1.9 Jy data (Dekel *et al.* 1993). Unfortunately, nonlinear biasing effects are hard to distinguish from non-linear gravitational effects, so a specific nonlinear biasing scheme is a prerequisite for such an analysis.

### 5.3. Simultaneous Fit of Velocity and Density: SIMPOT

The dynamical fields *and*  $\beta$  can be recovered simultaneously by a fit of a parametric model for the potential field to the combined data of the observed radial peculiar velocities and the distribution of galaxies in redshift space. This procedure takes advantage of the complementary features of the data in the recovery of the fields, it enforces the same effective smoothing on the data without preliminary reconstruction procedures such as POTENT, and it obtains a more reliable best fit by simultaneous rather than successive minimization. It has been implemented so far to the forward TF data, but it can be generalized in principle to minimize inverse TF residuals.

In the SIMPOT procedure by Nusser & Dekel (1997), the model for the potential field is taken to be an expansion in spherical harmonics  $Y_{lm}$  and Bessel functions  $j_l$  where the coefficients  $\Phi_{lmn}$  are the free parameters,

$$\Phi(\mathbf{r}) = \sum_{l=1}^{l_{max}} \sum_{m=-l}^l \sum_{n=1}^{n_{max}} \Phi_{lmn} j_l(k_n r) Y_{lm}(\hat{\mathbf{r}}). \quad (14)$$

The model radial velocity is derived from this potential by  $u = -\partial\Phi/\partial r$ , and the model density in redshift space is derived using linear theory via  $\delta = f^{-1}\nabla^2\Phi + s^{-2}(\partial/\partial s)(s^2\partial\Phi/\partial s)$ . The second term reflects redshift distortions, where  $s$  is the radial variable in redshift space. The resulting models for  $u(\mathbf{x})$  and  $\delta(\mathbf{s})$  are expansions in certain functions  $A_{lmn}$  and  $B_{lmn}$  that are appropriate combinations of the original base functions.

The combined  $\chi^2$  to minimize as a function of the parameters  $\Phi_{lmn}$  and  $\beta$  is the sum of

$$\chi_u^2 = \sum_i \sigma_{ui}^{-2} \left[ u_i^{obs} - \sum_{lmn} A_{lmn}(\mathbf{r}_i) \Phi_{lmn} \right]^2 \quad (15)$$

and

$$\chi_\delta^2 = \int d^3s \sigma_\delta^{-2}(\mathbf{s}) \left[ \delta^{obs}(\mathbf{s}) - \sum_{lmn} B_{lmn}(\mathbf{s}) \Phi_{lmn} \right]^2. \quad (16)$$

The observations are the peculiar velocities  $u_i^{obs}$  and a continuous density field in redshift space  $\delta^{obs}(\mathbf{s})$ , that is somewhat more tricky to obtain. The  $\beta$  dependence enters only in  $\chi_\delta^2$ , both via the velocity-density relation and the redshift distortions.

A SIMPOT fit to the Mark III peculiar velocity data and the IRAS 1.2 Jy redshift survey provides first hints for scale-dependent biasing:  $\beta_r \approx 0.6$  and  $1.0 (\pm 0.1)$  for smoothings that are roughly equivalent to Gaussian with radii 6 and  $12 h^{-1}\text{Mpc}$  respectively.

#### 5.4. Velocity-Velocity Comparison on Small Scales: VELMOD

Earlier comparisons of the peculiar velocities from the Mark II catalog and the velocities predicted from the IRAS redshift surveys (QDOT, 1.9 Jy, and 1.2 Jy) yielded estimates of  $\beta_I$  in the range 0.4 – 1.0 (Kaiser *et al.* 1991; Nusser & Davis 1994).

The more sophisticated recent VELMOD method of comparison (Willick *et al.* 1997b) compares the raw peculiar velocity data with a “model” velocity field that is predicted from the IRAS 1.2 Jy redshift survey. It is done without attempting to reconstruct a velocity field from the data. The key feature of VELMOD is that it explicitly allows for a non-unique mapping between real space and redshift space. Triple valuedness in the redshift field as well as non-negligible small-scale velocity “temperature” are treated in a unified way. This is done by expressing the probability that an object at distance  $r$  has a redshift  $z$  by

$$P(z|r) = \frac{1}{\sqrt{2\pi}\sigma_u} \exp \left[ -\frac{1}{2} \frac{[z - r - u(r)]^2}{2\sigma_u^2} \right] \quad (17)$$

where  $u(r)$  is the radial component of the model velocity field and  $\sigma_u$  is the small-scale velocity noise (which can in principle be a function of position). The above probability is then multiplied by the TF probability factor,  $P(m, \eta, r)$ , and integrated over the entire line-of-sight to obtain the probability of the *observable* quantities  $(m, \eta, z)$ . One then maximizes that probability over the entire data set.

The method is computer-intensive because numerical integrals are required for each galaxy, and for each fit parameter (TF parameters,  $\sigma_u$ , velocity field model parameters, etc.). This effort is worthwhile to the degree that the velocity field is triple-valued or the small-scale noise  $\sigma_u$  is comparable to the TF error. In particular, VELMOD is more rigorous in an analysis of the very local ( $z \leq 3000 \text{ km s}^{-1}$ ) region.

VELMOD has been applied with a Gaussian smoothing of  $3 h^{-1} \text{ Mpc}$  to the IRAS 1.2 Jy redshift survey and a subset of 838 spiral galaxies from the Mark III catalog within  $z \leq 3000 \text{ km s}^{-1}$  of the Local Group. The method was tested successfully using mock catalogs drawn from the N-body simulation of Kolatt *et al.* (1996). When applied to the real data it yielded consistency with the model of linear GI and linear biasing once an artificial quadrupole was allowed, with  $\beta_I = 0.5 \pm 0.1$  at  $3 h^{-1} \text{ Mpc}$ . The catch is that it is not at all clear why linear GI and the simplified deterministic biasing should be valid for the densities and velocities at such high resolution. The estimated value of  $\beta$  should therefore be interpreted with caution.

It is interesting to note that Shaya *et al.* (1995) obtained a similarly low value for  $\beta_o$  from the same local neighborhood. They applied the least-action reconstruction method to a redshift survey of several hundred spirals in comparison with TF data. Their method is likely to underestimate  $\beta$  because it assumes that the mass is all concentrated in the centers of galaxies and groups and thus tends to overestimate the gravitational forces between them. This systematic effect is yet to be quantified.

Table 1 summarizes the estimates of  $\beta$  and  $\Omega$  from cosmic flows.

Table 1:  $\Omega$  and  $\beta$  from Cosmic Flows

Peculiar Velocities Alone	Gaussian IPDF	Nusser & Dekel 93	$\Omega > 0.3 (> 4\sigma)$
	Skewness( $\nabla \cdot \mathbf{v}$ )	Bernardeau <i>et al.</i> 94	$\Omega > 0.3 (2\sigma)$
	Void	Dekel & Rees 94	$\Omega > 0.3 (2.4\sigma)$
	Power spectrum +COBE	Kolatt & Dekel 97 Zaroubi <i>et al.</i> 97a	$\sigma_8 \Omega^{0.6} = 0.7 \pm 0.15$ $\sigma_8 \Omega^{0.6} = 0.8 \pm 0.15$
Galaxy Density vs. Velocities	M2-QDOT $v$	Kaiser <i>et al.</i> 91	$\beta_I = 0.9^{+0.2}_{-0.15}$
	M3-I1.2 $v$ -dipole	Nusser & Davis 94	$\beta_I = 0.6 \pm 0.2$
	M3-I1.2 $v$ -inverse	Davis <i>et al.</i> 96	$\beta_I = 0.6 \pm 0.2(?)$
	M3-I1.2 $v$ G3	Willick <i>et al.</i> 96	$\beta_I = 0.5 \pm 0.1$
	M3-I1.2 $\delta$ G12	Sigad <i>et al.</i> 97	$\beta_I = 0.86 \pm 0.15$
	M3-I1.2 $\delta/v$ G6-12	Nusser & Dekel 96	$\beta_I = 0.6 - 1.0$ scale
	M2-Optical $v$	Hudson 94	$\beta_O = 0.5 \pm 0.1$
	TF-Optical	Shaya <i>et al.</i> 94	$\beta_O = 0.35 \pm 0.1$
	M3-Optical $\delta$ G12	Hudson <i>et al.</i> 95	$\beta_O = 0.75 \pm 0.2$
	M3-clusters G15	Plionis <i>et al.</i> 97	$\beta_C = 0.26 \pm 0.11$
Redshift Distortions	$\xi$ I1.2	Peacock & Dodds 94	$\beta_I = 1.0 \pm 0.2$
	$\xi$ I1.2	Fisher <i>et al.</i> 94a	$\beta_I = 0.45^{+0.3}_{-0.2}$
	$Y_{lm}$ I1.2	Fisher <i>et al.</i> 94b	$\beta_I = 1.0 \pm 0.3$
	$P_k$ I1.2, QDOT	Cole <i>et al.</i> 95	$\beta_I = 0.5 \pm 0.15$
	$\xi$ I1.2, QDOT	Hamilton 95	$\beta_I = 0.7 \pm 0.2$
	$Y_{lm}$ I1.2	Heavens & Taylor 95	$\beta_I = 1.1 \pm 0.3$
	$P_k$ I1.2	Fisher & Nusser 96	$\beta_I = 0.6 \pm 0.2$
CMB Dipole	vs galaxies angular	Yahil <i>et al.</i> 86	$\beta_I = 0.9 \pm 0.2$
	vs galaxies redshift	Strauss <i>et al.</i> 92	$\beta_I = 0.4 - 0.85$
		Rowan-Rob. <i>et al.</i> 91	$\beta_I = 0.8^{+0.2}_{-0.15}$
	vs galaxies angular	Lynden-Bell <i>et al.</i> 89	$\beta_O = 0.3 - 0.5$
	vs galaxies redshift	Hudson 93	$\beta_O = 0.7^{+0.4}_{-0.2}$
	clusters	Scaramella <i>et al.</i> 91	$\beta_C \sim 0.13$
	Plionis <i>et al.</i> 91	$\beta_C \sim 0.17 - 0.22$	

$$\beta \equiv \Omega^{0.6}/b, \quad b_C : b_O : b_I \approx 4.5 : 1.3 : 1.0, \quad \sigma_8 \Omega^{0.6} = (0.69 \pm 0.05)\beta_I,$$

M3= Mark III, I1.2 = IRAS 1.2 Jy, G12 = Gaussian smoothing  $12 h^{-1}$ Mpc

### 5.5. Galaxy Biasing as a Stochastic Process

In all the methods described in § 5, the cosmological parameter of interest  $\Omega$  is contaminated by the uncertain relation between galaxy and mass density, the so called “galaxy biasing”. Nontrivial galaxy biasing clearly exists. The fact that galaxies of different types cluster differently (Dressler 1980) implies that at least some do not trace the underlying mass. This is hardly surprising because any reasonable physical theory would predict non-trivial biasing (Kaiser 1984; Davis *et al.* 1985; Bardeen *et al.* 1986; Dekel & Silk 1986; Dekel & Rees 1987; Braun, Dekel & Shapiro 1988; Weinberg 1995). In particular, simulations of galaxy formation in a cosmological context (*e.g.*, Cen & Ostriker 1992; 1993; Lemson *et al.* 1997) indicate a biasing relation that is non-linear in density, is varying with scale, and has a statistical scatter reflecting dependencies on factors other than density.

One should therefore not be surprised by the fact that the various estimates of  $\beta$  span a large range, from less than one half to more than unity. Some of this scatter is due to the different types of galaxies involved, and some may be due to remaining effects of non-linear gravity or other systematic errors, but a significant fraction of the scatter in  $\beta$  is likely to reflect non-trivial properties of the biasing scheme. This means that translating a measured  $\beta$  into  $\Omega$  is non-trivial; it requires a detailed knowledge of the relevant biasing scheme.

In order to strengthen this point, we demonstrate below that an obvious source of systematic variations in  $\beta$  is the inevitable *statistical* scatter in the biasing process (Dekel & Lahav 1997). This scatter in the relation between densities can be interpreted as reflecting the dependence of galaxy formation efficiency, or galaxy density, on physical properties of the protogalaxy environment other than density. These could be local properties such as the potential field, the deformation tensor, tidal effects, and angular momentum, or long-range effects carried by radiation or particles from neighboring sources. In the simple example below, we assume that this scatter in the biasing is local and neglect possible spatial correlations.

Let  $\delta(\mathbf{x})$  be the field of mass-density fluctuations smoothed with a given window, and let  $\delta_G(\mathbf{x})$  be the corresponding field for galaxies of a given type. We treat them as random fields, both with probability densities of zero mean by definition. Denote  $\langle \delta^2 \rangle \equiv \sigma^2$  and  $\langle \delta^3 \rangle \equiv S$ . Consider the “biasing” relation between galaxies and mass to be a *random* process, specified by the *conditional probability* function  $B(\delta_G|\delta)$ . The common deterministic biasing relation,  $\delta_G = b(\delta)\delta$ , is replaced by the conditional mean,

$$\langle \delta_G | \delta \rangle \equiv b(\delta)\delta. \tag{18}$$

The statistical character of the relation is expressed by the conditional moments of higher order about the mean, such as

$$\langle (\delta_G - b\delta)^2 | \delta \rangle \equiv \sigma_b^2, \quad \text{and} \quad \langle (\delta_G - b\delta)^3 | \delta \rangle \equiv S_b. \tag{19}$$

This statistical nature of biasing leads to a different “biasing parameter” for each specific application.

Take for example the ratio of variances,  $b_2^2 \equiv \langle \delta_G^2 \rangle / \langle \delta^2 \rangle$ , such as being obtained by a ratio of power spectra or two-point correlation functions, or by comparing the mass function of clusters to the variance of  $\delta_G$  at  $8 h^{-1} \text{Mpc}$  (White, Efstathiou & Frenk 1993). One can prove in general that  $\langle \delta_G^m \rangle = \langle \langle \delta_G^m | \delta \rangle_{\delta_G} \rangle_{\delta}$ , and therefore,  $\langle \delta_G^2 \rangle = \langle b^2(\delta) \delta^2 \rangle + \langle \sigma_b^2(\delta) \rangle$ . Thus, in the simple case where  $b(\delta)$  is constant,  $b_2$  is an overestimate of  $b$  by

$$b_2 = b(1 + \Delta_2)^{1/2}, \quad \Delta_2 \equiv \langle \sigma_b^2 \rangle / (\sigma^2 b^2). \quad (20)$$

Another common way of estimating  $\beta$  is via linear regression of the noisy field  $-\nabla \cdot \mathbf{v}(\mathbf{x})$  [ $\approx f(\Omega)\delta(\mathbf{x})$ ] on  $\delta_G(\mathbf{x})$  (§ 5.2), or via a regression of the corresponding velocities. The slope of the forward regression of  $\delta_G$  on  $\delta$  is  $b_f = \langle \delta_G \delta \rangle / \langle \delta^2 \rangle$ , and the slope of the inverse regression of  $\delta$  on  $\delta_G$  is  $b_i^{-1} = \langle \delta \delta_G \rangle / \langle \delta_G^2 \rangle$ . In the case where  $b$  is constant,  $b_f = b$ , and  $b_i$  is an overestimate,

$$b_i = b(1 + \Delta_2). \quad (21)$$

The promising method of estimating  $\beta$  from large-scale redshift distortions measures yet a different quantity. It turns out that most methods for determining  $\beta$  lead similarly to an underestimate.

The level of the effect depends on the actual values of  $\Delta_2$  and similar parameters. One way to estimate the natural biasing scatter at a given smoothing scale is by investigating goodness of fit of the density fields of mass and light and the model of deterministic biasing. By requiring that  $\chi^2 = 1$  per degree of freedom one can estimate the scatter needed in addition to the known errors. For example, Hudson *et al.* (1995) estimated for optical galaxies versus POTENT Mark III mass at  $12 h^{-1} \text{Mpc}$  smoothing  $\sigma_b \sim 0.15$ , which corresponds to  $\Delta_2 \sim 0.25$ . Alternatively, one can estimate  $\sigma_b$  from theoretical simulations. For example, preliminary hydro simulations (Cen & Ostriker 1993) yield  $\sigma_b = 0.25$  under  $10 h^{-1} \text{Mpc}$  Gaussian smoothing, i.e.  $\Delta_2 \sim 0.4$ . If  $b = \Omega = 1$ , then the  $\beta$  values derived by the various methods are expected to span the range  $0.7 \leq \beta \leq 1$ , and this is solely due to the dispersion in the biasing relation. A large skewness in  $B(\delta_G | \delta)$  may stretch this range even further.

A relevant moral from the biasing uncertainty is that methods for measuring  $\Omega$  independent of density biasing (§ 4) are desirable. However, it has to be born in mind that the galaxies may also be biased tracers of the *velocity* field of the matter. Such a “velocity biasing” would affect any attempt to extract dynamical information from large-scale velocities. The expected magnitude of the velocity biasing in the standard scenarios of structure formation is a matter of debate, and even it’s sign is unclear (*e.g.*, Summers *et al.* 1995). Based on recent simulations it seems likely to be limited to a  $\sim 10 - 20\%$  effect.

## 6. COSMOLOGICAL PARAMETERS

The previous sections discussed measurements of the mass-density parameter  $\Omega$  (directly or via  $\beta$ ) from large-scale structure on scales  $10 - 100 h^{-1} \text{Mpc}$ . In this section we try to put these estimates in a wider perspective (see Dekel, Burstein & White 1997 for a review).



One very interesting large-scale constraint that has not been discussed here is based on cluster abundance, that can be predicted for a Gaussian field via the Press-Schechter formalism, and is quite insensitive to the shape of the power spectrum. The current estimates are  $\sigma_8\Omega^{0.6} \simeq 0.5 - 0.6$  (White, Efstathiou & Frenk 1993; Eke *et al.* 1996; Mo *et al.* 1996). This is only slightly lower than the estimates of  $\sigma_8\Omega^{0.6} \simeq 0.7 - 0.8$  from the power spectrum of the peculiar velocity data (§ 3.2, § 3.3). Note that this quantity is related to  $\beta_I$  via  $\sigma_8\Omega^{0.6} = \sigma_{8I}\beta_I$ , where  $\sigma_{8I}$  is the rms fluctuation of IRAS galaxies in a top hat window of  $8 h^{-1}\text{Mpc}$ . With the estimate from the IRAS 1.2 Jy survey of  $\sigma_{8I} = 0.69 \pm 0.05$  (Fisher *et al.* 1994a), the results from cluster abundance and from the  $\delta - \delta$  POTENT-IRAS comparison (§ 5.2) are in pleasant agreement.

Constraints from virialized systems such as galaxies and clusters on smaller comoving scales of  $1 - 10 h^{-1}\text{Mpc}$  (*e.g.*, Primack 1997; Bahcall 1997; Peebles 1997) typically yield low values of  $\Omega \sim 0.2 - 0.3$ , but with several loopholes. Most interesting among these is the constraint involving the baryonic fraction in clusters from X-ray data and the estimates of  $\Omega_b$  from the observed deuterium abundance and the theory of big-bang nucleosynthesis. With baryonic fraction in the middle of the observed range  $f_b = (0.03 - 0.08)h^{-3/2}$  (White *et al.* 1993; White & Fabian 1995), and with the recent estimates of  $\Omega_b h^2 \simeq 0.025$  (Tytler *et al.* 1996; Burles & Tytler 1996), the current estimate is  $\Omega \simeq 0.5h_{65}^{-1/2}$ . This result favors a low value of  $\Omega$ , but  $\Omega = 1$  cannot be definitively excluded.

The global cosmological measures commonly involve combinations of the cosmological parameters, such as the mass  $\Omega$  ( $\equiv \Omega_m$ ) and the contribution of the vacuum energy density  $\Omega_\Lambda$ . Constraints in the  $\Omega - \Omega_\Lambda$  plane are displayed in Figure 15, and briefly discussed below.

**Occam’s Razor.** The above working hypotheses, and the order by which more specific models should be considered against observations, are guided by the principle of Occam’s Razor, *i.e.*, by simplicity and robustness to initial conditions. It is commonly assumed that the simplest model is the Einstein-deSitter model,  $\Omega = 1$  and  $\Omega_\Lambda = 0$ . One property that makes it robust is the fact that  $\Omega$  remains constant at all times with no need for fine tuning at the initial conditions. The most natural extension according to the generic model of inflation is a flat universe,  $\Omega_{tot} = 1$ , where  $\Omega$  can be smaller than unity but only at the expense of a nonzero cosmological constant.

**Classical Tests of Geometry.** The parameter-dependent large-scale geometry of space-time is reflected in the volume-redshift relation. There are two classical versions of the tests that utilize this dependence: magnitude versus redshift (or “Hubble diagram”) and number density versus redshift. The luminosity distance and the angular-diameter distance to a redshift  $z$ , which enter these tests, depend on  $\Omega$  and  $\Omega_\Lambda$ . At  $z \sim 0.4$ , these distances happen to be (to a good approximation) a function of the combination  $\Omega - \Omega_\Lambda$  (not  $q_0$ ) (Perlmutter *et al.* 1996).

The main advantage of such tests is that they are direct measures of global geometry. Supernovae type Ia are the popular current candidate for a standard candle, based on the assumption that stellar processes are not likely to vary much in time.

The first 7 supernovae analyzed by Perlmutter *et al.* (1996) at  $z \sim 0.4$  yield  $-0.3 <$

$\Omega - \Omega_\Lambda < 2.5$  as the 90% two-parameter likelihood contour (Fig. 15). For a *flat* universe they find for each parameter  $\Omega = 0.94_{-0.28}^{+0.34}$ , and  $\Omega_\Lambda < 0.51$  (or equivalently  $\Omega > 0.49$ ) at 95% confidence.

**Number Count of Quasar Lensing.** This is a promising new version of the classical number density test. When  $\Omega_\Lambda$  is positive and comparable to  $\Omega$ , the universe should have gone through a phase of slower expansion in the recent cosmological past, which should be observed as an accumulation of objects at a specific redshift of order unity. In particular, it should be reflected in the observed rate of lensing of high-redshift quasars by foreground galaxies (Fukugita *et al.* 1990). The contours of constant lensing probability in the  $\Omega - \Omega_\Lambda$  plane for  $z_s \sim 2$  happen to almost coincide with the lines  $\Omega - \Omega_\Lambda = \text{const}$ . The limits from lensing are thus similar in nature to the limits from SNe Ia.

This test shares all the advantages of direct geometrical measures. The high redshifts involved bring about a unique sensitivity to  $\Omega_\Lambda$ , compared to the negligible effect that  $\Omega_\Lambda$  has on the structure observed at  $z \ll 1$ .

From the failure to detect the accumulation of lenses, the current limit for a *flat* model is  $\Omega_\Lambda < 0.66$  (or  $\Omega > 0.36$ ) at 95% confidence (Kochanek 1996) (Fig. 15).

**Microwave Background Acoustic Peaks.** This test is expected to provide the most stringent constraints on the cosmological parameters within a decade. The next generation of CMB satellites (MAP, to be launched by NASA in 2001, and in particular Planck, scheduled by ESA for 2004) are planned to obtain a precision at  $\sim 10$  arc-minute resolution that will either rule out the current framework of GIf for structure formation or will measure the cosmological parameters to high precision. Detailed evaluation of Planck shows that nominal performance and expected foreground subtraction noise will allow parameter estimation with the following accuracy (ignoring systematics):  $H_0 \pm 1\%$ ,  $\Omega_{tot} \pm 0.005$ ,  $\Omega_\Lambda \pm 0.02$ ,  $\Omega_b \pm 2\%$ .

Current ground-based and balloon-born experiments provide preliminary constraints on the *location* of the first acoustic peak on sub-degree scales in the angular power spectrum of CMB temperature fluctuations,  $l(l+1)C_l$ . In the vicinity of a flat model, the first peak is predicted at approximately the multipole  $l_{peak} \simeq 220(\Omega + \Omega_\Lambda)^{-1/2}$ . The results of COBE’s DMR ( $l \sim 10$ ) provide an upper bound of  $\Omega + \Omega_\Lambda < 1.5$  at the 95% confidence level for a scale-invariant initial spectrum (and the constraint becomes tighter for any “redder” spectrum,  $n < 1$ ) (White & Scott 1996). Several balloon experiments ( $l \sim 50 - 200$ ) strengthen this upper bound (*e.g.*, the Saskatoon experiment, Scott *et al.* 1996). The Saskatoon experiment and the CAT experiment ( $l \sim 350 - 700$ ) yield a preliminary lower bound of  $\Omega + \Omega_\Lambda > 0.3$  (Hancock *et al.* 1996) (Fig. 15).

**The Age of the Universe.** Measured independent lower bounds on the Hubble constant and on the age of the oldest globular clusters provide a lower bound on  $H_0 t_0$  ( $= 1.05ht$ , where  $H_0 \equiv 100h \text{ km s}^{-1} \text{ Mpc}^{-1}$  and  $t_0 \equiv 10t \text{ Gyr}$ ), and thus an interesting constraint in the  $\Omega - \Omega_\Lambda$  plane. The exact expressions are computable in the various regions of parameter space. A useful crude approximation near  $H_0 t_0 \sim 2/3$  is  $\Omega - 0.7\Omega_\Lambda \simeq 5.8(1 - 1.3ht)$ .

Progress has been made in measuring  $H_0$  via the HST key project detecting Cepheids in nearby clusters for calibration of TF distances, and via accurate distances to SNe Type

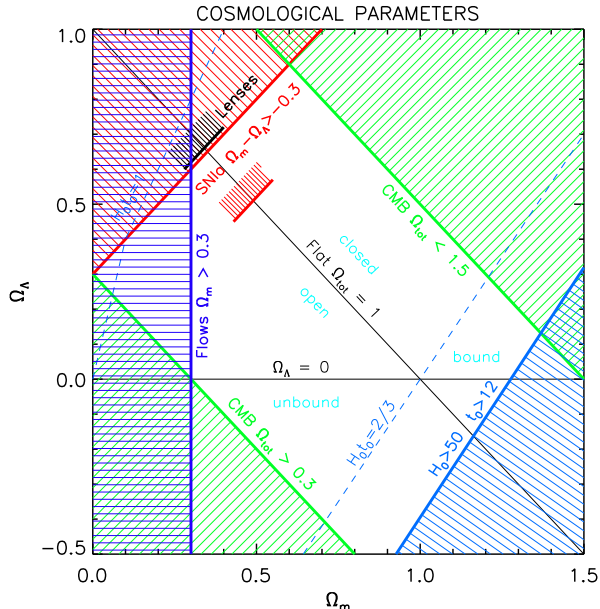


Fig. 15.— Current limits ( $\sim 2\sigma$ ) on the cosmological parameters  $\Omega$  and  $\Omega_\Lambda$  from global measures: luminosity distance of SNIa, lens count, the location of the CMB peak, and the age versus Hubble constant. The short marks are the one-parameter 95% limits from SNIa and lenses for a flat universe. Also shown (vertical line) is the 95% lower bound on  $\Omega$  from cosmic flows. The most likely value of  $\Omega$  lies in the range 0.5 to 1. The Einstein-deSitter model is permitted. An open model with  $\Omega \simeq 0.2$  and  $\Omega_\Lambda = 0$ , or a flat model with  $\Omega \simeq 0.3$  and  $\Omega_\Lambda \simeq 0.7$ , are ruled out (Dekel, Burstein & White 1997).

Ia. The new calibration of local Cepheids by the Hipparcos astrometric satellite (Feast & Catchpole 1997) seem to have reduced the estimates of  $H_0$  by  $\sim 10\%$ . The indications from SNe velocities for a local void of radius  $\sim 75 h^{-1}\text{Mpc}$  out to the Great Wall (Zehavi *et al.* 1997), takes another  $\sim 5\%$  from  $H_0$  as measured by TF distances from within the void, and brings the various estimates into agreement at  $h \simeq 0.6 \pm 0.1$ .

The Hipparcos calibration of the distances to local subdwarf stars (Reid 1997) had an even more dramatic effect on the estimates of the ages of the oldest globular clusters (*e.g.*, Van den Berg *et al.* 1996). The current estimates seem to be  $t \simeq 1.2 \pm 0.2$  (*e.g.*, M. Bolte, private communication). Thus, the most likely value of  $H_0 t_0$  is not far from  $2/3$ , consistent with the standard Einstein deSitter model.

## 6.1. Conclusion

We conclude with a summary of the main implications of the observed cosmic flows.

**Gravitational Instability.** The strongest evidence for gravitational origin of structure comes from the growth rate of fluctuations as indicated by the comparison of the  $\delta T/T \sim 10^{-5}$  fluctuations at the last scattering surface and the  $\sim 300 \text{ km s}^{-1}$  motions over  $\sim 100 h^{-1}\text{Mpc}$

scales in our local neighborhood.

**Initial fluctuations and Dark Matter.** The COBE measurements of CMB fluctuations at large angular scales and the comparison to the observed flows indicate a power spectrum near scale invariance,  $n \sim 1$ .

The bulk velocity in a sphere of radius  $50 h^{-1}\text{Mpc}$  about the LG is  $V_{50} = 375 \pm 85 \text{ km s}^{-1}$ . The mass power spectrum deduced from the peculiar velocities has an amplitude of  $P_{0.1}\Omega^{1.2} = (5 \pm 2) \times 10^3 (h^{-1}\text{Mpc})^3$  at  $k = 0.1 (h^{-1}\text{Mpc})^{-1}$ . This extrapolates to  $\sigma_8\Omega^{0.6} = 0.8 \pm 0.2$  on smaller scales.

For COBE-normalized CDM models, a likelihood analysis of the mass power spectrum yields  $\Omega n^2 h_{65} = 0.7 \pm 0.2$ . A comparison to preliminary detections of the first acoustic peak in the CMB angular power spectrum requires that  $n \gtrsim 0.9$ , and that  $\Omega_b \sim 0.1$ . Thus, within the family of CDM models, most successful in matching the current LSS data are either of the following variants: (a)  $\Omega = 1$  with a tilted spectrum  $n \sim 0.9$ , (b)  $\Omega \sim 0.5$ , with or without a cosmological constant, and  $n = 1$ , and (c)  $\Omega = 1$  with 20% hot dark matter. A high baryonic content (and relatively low  $\Omega$ ) may be required to explain a peak in the galaxy density power spectrum at  $\sim 125 h^{-1}\text{Mpc}$ , if confirmed (Broadhurst *et al.* 1990; S. Landy based on LCRS, private communication; Cohen *et al.* 1996; Einasto 1997).

In view of the nucleosynthesis constraints on the baryonic density, the high  $\Omega$  indicated by the motions requires non-baryonic dark matter. The observed mass-density power spectrum on scales  $10\text{--}100 h^{-1}\text{Mpc}$  does not yet allow a clear distinction between the competing models involving baryonic, cold and hot dark matter and possibly a cosmological constant. I do not think that any of the front-runner models can be significantly ruled out based on current tests, contrary to occasional premature statements in the literature about the “death” of a certain model. I predict that were the dark matter constituent(s) to be securely detected in the lab, the corresponding scenario of LSS would find a way to overcome the  $\sim 2\sigma$  obstacles it may be facing now.

**Galaxy Biasing and  $\beta$ .** Generally speaking, galaxies trace mass. For each of the different smoothing scales, the data of velocities and redshift surveys are consistent with GI and linear biasing (properly modified in the tails). However, the best estimates of  $\beta_l$  span the range  $0.5 - 1.0$ . This can be explained by the fact that, when inspected in detail, the biasing scheme involves scale dependence, non-linear features, and intrinsic scatter. It is difficult to distinguish non-linear biasing from non-linear gravitational effects.

**The Value of  $\Omega$ .** Methods based on virialized objects tend to favor low values of  $\Omega \sim 0.2$ , but with plausible loopholes.

The current peculiar-velocity data provide in several different ways a significant ( $> 2\sigma$ ) lower bound of  $\Omega > 0.3$ . This bound is independent of  $\Lambda$ ,  $H_0$ , and the biasing relation between galaxies and mass. The range of  $\beta$  values obtained on different scales by different methods may be partly due to underestimated errors and partly due to non-trivial biasing.

The global measures of geometry provide a lower bound of similar nature,  $\Omega - \Omega_\Lambda > 0.3$ . The age constraints, which used to favor low values of  $\Omega$  until recently, seem to agree with

$\Omega \sim 1$  according to the new calibration of the distance scale by Hipparcos.

The data is thus consistent with  $\Omega = 1$ . Based on the whole range of constraints, and ignoring the Occam's razor desire for simplicity, the most likely value may be argued to be  $\Omega \sim 0.5$ . Values of  $\Omega = 0.3$  and below are significantly ruled out. The data are consistent with the general predictions of Inflation: flat geometry and Gaussian, almost scale-invariant initial fluctuations.

### Acknowledgments:

This review is based on work with several close collaborators (see references), supported by grants from the US-Israel Binational Science Foundation, the Israel Science Foundation, the NSF and NASA.

### REFERENCES

- Aaronson, M., Huchra, J., Mould, J. R., Tully, R. B., & Fisher, J. R., *et al.* 1982a, ApJS, 50, 241  
Babul, A., Weinberg, D., Dekel, A., & Ostriker, J. P. 1994, ApJ, 427, 1  
Bahcall, N. 1997, in Formation of Structure in the Universe, eds. A. Dekel & J.P. Ostriker (Cambridge Univ. Press) (astro-ph/9611148) in press  
Bardeen, J., Bond, J. R., Kaiser, N., & Szalay, A. 1986, ApJ, 304, 1  
Bernardeau, F. 1992, ApJ, 390, L61  
Bernardeau, F., Juszkiewicz, R., Dekel, A., & Bouchet, F., 1995, MNRAS, 274, 20  
Bertschinger, E., Dekel, A. 1989, ApJ, 336, L5  
Bertschinger, E., Dekel, A., Faber, S.M., Dressler, A., & Burstein, D. 1990, ApJ, 364, 370  
Bertschinger, E., Gorski, K., & Dekel, A. 1990, Nature, 345, 507  
Blumenthal, G. R., Dekel, A., & Yahil, A. 1997, in preparation  
Bouchet, F., Juszkiewicz, R., Colombi, S., & Pellat, R. 1992, ApJ, 394, L5  
Braun, E., Dekel, A., & Shapiro, P. 1988, ApJ, 328, 34  
Broadhurst, T. J., Ellis, R. S., Koo, D. C., & Szalay, A. S. 1990, Nature, 343, 726  
Burles, S., & Tytler, D. 1996, ApJ, 460, 584  
Cen, R., & Ostriker, J. P. 1992, ApJ, 399, L113  
Cen, R., & Ostriker, J. P. 1993, ApJ, 417, 415  
Cohen, J. G., Cowie, L. L., Hogg, D. W., Songaila, A., Blandford, R., Hu, E. M., & Shopbell, P. 1996, ApJ, 471, 5  
Cole, S., Fisher, K. B., & Weinberg, D. 1995, MNRAS, 275, 515  
Courteau, S., Faber, S. M., Dressler, A., & Willick J. A. 1993, ApJ, 412, L51  
da Costa, L.N., Freudling, W., Wegner, G., Giovanelli, R., Haynes, M., Salzer, J.J. 1996, ApJ, 468, L5

- Davis, M., Efstathiou, G., Frenk, C. S., & White, S. D. M. 1985, *ApJ*, 292, 371
- Davis, M., Nusser, A., & Willick, J. A. 1996, *ApJ*, 473, 22
- Dekel, A. 1981, *A&A*, 101, 79
- Dekel, A. 1994, *ARA&A*, 32, 371
- Dekel, A. 1997, in *Formation of Structure in the Universe*, eds. A. Dekel & J.P. Ostriker (Cambridge Univ. Press) in press
- Dekel, A., Bertschinger, E., & Faber, S.M. 1990, *ApJ*, 364, 349
- Dekel, A., Bertschinger, E., Yahil, A., Strauss, M., Davis, M., & Huchra, J. 1993, *ApJ*, 412, 1
- Dekel, A., Burstein, D., & White, S. D. M. 1997, in *Critical Dialogs in Cosmology*, ed. N. Turok (Princeton: Princeton University Press) in press (astro-ph/9611108)
- Dekel, A., Eldar, A., Kolatt, T., Yahil, A., Willick, J.A., Faber, S.M., Courteau, S., & Burstein, D. 1997, *ApJ*, , in preparation
- Dekel, A., & Lahav, O. 1997, in preparation
- Dekel, A., & Rees, M. J. 1987, *Nature*, 326, 455
- Dekel, A., & Rees, M. J. 1994, *ApJ*, 422, L1
- Dekel, A., & Silk, J. 1986, *ApJ*, 303, 39
- Dressler, A. 1980, *ApJ*, 236, 351
- Dressler, A., Lynden-Bell, D., Burstein, D., Davies, R. L., Faber, S. M., Terlevich, R., & Wegner, G. 1987, *ApJ*, 313, 42
- Einasto, J. *et al.* 1997, *Nature*, 385, 139
- Eke, V. R., Cole, S., & Frenk, C. S. 1996, astro-ph 9601088
- Eldar, A., Dekel, A., & Willick, J. A. 1997, in preparation
- Feast, M. W., & Catchpole, R. M. 1997, *MNRAS*, , submitted
- Fisher, K. B., Davis, M., Strauss, M. A., Yahil, A., & Huchra, J. P. 1994a, *MNRAS*, 266, 50
- Fisher, K. B., Davis, M., Strauss, M. A., Yahil, A., & Huchra, J. P. 1994b, *MNRAS*, 267, 92
- Fisher, K. B., & Nusser, A. 1996, *MNRAS*, 279, L1
- Fukugita, M., Yamashita, K., Takahara, F., & Yoshii, Y. 1990, *ApJ*, 361, L1
- Ganon, G., Dekel, A., Mancinelli, P., & Yahil, A. 1997, in preparation
- Giovanelli, R. *et al.* 1997, in preparation
- Gramman, M. 1993, *ApJ*, 405, L47
- Hamilton, A. J. S. 1995, in *Clustering in the Universe*, eds. C. Balkowski & S. Morgatadeau (Editions Frontieres)
- Hancock, S., Rocha, G., Lasenby, A. N., & Cutierrez, C. M. 1996, *MNRAS*, , submitted
- Heavens, A.F., & Taylor, A.N. 1995, *MNRAS*, 275, 483
- Hudson, M.J. 1993, *MNRAS*, 265, 72
- Hudson, M. J. 1994, *MNRAS*, 266, 475
- Hudson, M. J., Dekel, A., Courteau, S., Faber, S. M., & Willick, J. A. 1995, *MNRAS*, 274, 305
- Ikeuchi, S. 1981, *PASJ*, 33, 211
- Jaffe, A. H., & Kaiser, N. 1995, *ApJ*, 455, 26
- Kaiser, N. 1988, *MNRAS*, 231, 149

- Kaiser, N. 1984, ApJ, 284, L9
- Kaiser, N., Efstathiou, G., Ellis, R., Frenk, C., Lawrence, A., Rowan-Robinson, M., & Saunders, W. 1991, MNRAS, 252, 1
- Kochanek, C. S. 1996, ApJ, 466, 638
- Kofman, L., Bertschinger, E., Gelb, J., Nusser, A., & Dekel, A. 1994, ApJ, 420, 44
- Kolatt, T. & Dekel, A. 1994, ApJ, 428, 35
- Kolatt, T. & Dekel, A. 1997, ApJ, in press (astro-ph/9512132)
- Kolatt, T., Dekel, A., Ganon, G., & Willick, J. 1996, ApJ, 458, 419
- Kolatt, T., Dekel, A., & Primack, J. R. 1997, in preparation
- Landy, S., & Szalay, A. 1992, ApJ, 391, 494
- Lauer, T.R., & Postman, M. 1993, ApJ, 425, 41
- Lemson, G., Dekel, A., Kauffmann, G., & White, S. D. M. 1997, in preparation
- Lynden-Bell, D., Faber, S. M., Burstein, D., Davies, R. L., Dressler, A., Terlevich, R. J., & Wegner, G. 1988, ApJ, 326, 19
- Lynden-Bell, D., Lahav, O., & Burstein, D. 1989, MNRAS, 241, 325
- Mathewson, D. S., Ford, V. L., & Buchhorn, M. 1992, ApJS, 81, 41
- Mo, H. J., Jing, Y. P., & White, S. D. M. 1996, MNRAS, 282, 1096
- Nusser, A., & Dekel, A. 1992, ApJ, 391, 443
- Nusser, A., & Dekel, A. 1993, ApJ, 405, 43
- Nusser, A., & Dekel, A. 1997, in preparation
- Nusser, A., Dekel, A., Bertschinger, E., & Blumenthal, G.R. 1991, ApJ, 379, 6
- Nusser, A., Dekel, A., & Yahil, A. 1995, ApJ, 449, 439
- Ostriker, J. P., & Cowie, L. L. 1981, ApJ, 243, L127
- Peacock, J. A., & Dodds, S.J. 1994, MNRAS, 267, 102
- Peebles, P. J. E. 1997, in Formation of Structure in the Universe, eds. A. Dekel & J.P. Ostriker (Cambridge Univ. Press) in press
- Perlmutter, S., Gabi, S., Goldhaber, G. *et al.* 1996, ApJ, , submitted (astro-ph/9602122)
- Plionis, M., Branchini, E., Zehavi, I., & Dekel, A. 1997, in preparation
- Primack, J. R. 1997, in Formation of Structure in the Universe, eds. A. Dekel & J.P. Ostriker (Cambridge Univ. Press) in press
- Reid, I. N. 1997, ApJ, , submitted
- Riess, A. G., Press, W. H., & Kirshner, R. P. 1995, ApJ, 438, L17
- Rowan-Robinson, M., Lawrence, A., Saunders, W., & Leech, K. 1991, MNRAS, 253, 485
- Sachs, R. K., & Wolfe, A. M. 1967, ApJ, 147, 73
- Scaramella, R., Vettolani, G., & Zamorani, G. 1991, ApJ, 376, L1
- Schechter, P. 1980, AJ, 85, 801
- Scott P. F., Saunders, R., Pooley, G. *et al.* 1996, ApJ, 461, L1
- Shaya, E. J., Peebles, P. J. E., & Tully, R. B. 1995, ApJ, 454, 15
- Sigad, Y., Dekel, A., Strauss, M. S., & Yahil, A. 1997, in preparation

- Strauss, M. A. 1997, in *Formation of Structure in the Universe*, eds. A. Dekel & J.P. Ostriker (Cambridge Univ. Press) in press (astro-ph/9610033)
- Strauss, M. A., Cen, R., Ostriker, J. P., Lauer, T. R., & Postman, M. 1995, *ApJ*, 444, 507
- Strauss, M. A., Yahil, A., Davis, M., Huchra, J. P., & Fisher, K. B. 1992. *ApJ*, 397, 395
- Strauss, M. A., & Willick, J. A. 1995, *PhR*, 261, 271
- Sugiyama, N. 1995, *ApJS*, 100, 281
- Summers, F. J., Davis, M., & Evrard, A. E. 1995, *ApJ*, 454, 1
- Tytler, D., Fan, X. M., & Burles, S. 1996, *Nature*, 381, 207
- Van den Berg, D., Stetson, P., & Bolte, M. 1996, *ARA&A*, 34, 461
- Watkins, R., & Feldman, H. A. 1995, *ApJ*, 453, 73
- Weinberg, D. 1995, in *Wide-Field Spectroscopy and the Distant Universe*, eds. S.J. Maddox & A. Aragon-Salamanca (World Scientific: Singapore)
- White, M., & Scott, D. 1996, *ApJ*, 459, 415
- White, S. D. M., Efstathiou, G., & Frenk, C. S. 1993, *MNRAS*, 262, 1023
- White, S. D. M., Navarro, J., Evrard, A., & Frenk, C. S. 1993, *Nature*, 366, 429
- White, S. D. M., & Fabian, A. 1995, *MNRAS*, 273, 72
- Willick, J. 1994, *ApJS*, 92, 1
- Willick, J.A. 1997, in *Formation of Structure in the Universe*, eds. A. Dekel & J.P. Ostriker (Cambridge Univ. Press) in press (astro-ph/9610200)
- Willick, J.A., Courteau, S., Faber, S.M., Burstein, D., & Dekel, A. 1995, *ApJ*, 446, 1
- Willick, J.A., Courteau, S., Faber, S.M., Burstein, D., Dekel, A., & Kolatt, T. 1996, *ApJ*, 457, 460
- Willick, J.A., Courteau, S., Faber, S.M., Burstein, D., Dekel, A., & Strauss, M.A. 1997a, *ApJS*, in press (astro-ph/9610202)
- Willick, J.A., Strauss, M.S., Dekel, A., & Kolatt, T. 1997, *ApJ*, in press (astro-ph/9612240)
- Yahil, A., Walker, X., & Rowan-Robinson, M. 1986, *ApJ*, 301, L1
- Zaroubi, S., Hoffman, Y., & Dekel, A. 1997, in preparation
- Zaroubi, S., Sugiyama, N., Silk, J., Hoffman, Y., & Dekel, A. 1997b, *ApJ*, submitted (astro-ph/9610132)
- Zaroubi, S., Zehavi, I., Dekel, A., Hoffman, Y., & Kolatt, T. 1997a, *ApJ*, in press (astro-ph/9610226)
- Zehavi, I., Riess, A., Kirshner, R., & Dekel, A. 1997, in preparation
- Zel'dovich, Ya.B. 1970, *A&A*, 5, 20